Self-adaptive F.E.M.Algorithms for the Euler equations

Bernadette Palmerio

INRIA

CENTRE
SOPHIA ANTIPOLIS

Institut National
de Recherche
en Informatique
et en Automatique

Domaine de Voluceau
Rocquencourt
BP 105
78153 Le Chesnay Cedex
France
Tél. (3) 954 90 20

Rapports de Recherche

N° 338

SELF-ADAPTIVE F. E. M. ALGORITHMS FOR THE EULER EQUATIONS

Bernadette PALMERIO

Septembre 1984

SELF - ADAPTIVE F.E.M. ALGORITHMS FOR THE EULER EQUATIONS

Bernadette PALMERIO

Institut de Mathématiques et Sciences Physiques,
Parc Valrose, 06034 NICE CEDEX

et

INRIA, Route des Lucioles
Sophia Antipolis, 06560 VALBONNE

ABSTRACT :

We consider two-dimensional steady flows about airfoils of a compressible, inviscid fluid governed by the Euler Equations. Thus, the solution may present singularities such as stagnation points or shocks. In this work, a finite-element method based on triangular elements is presented that includes a self-adaptive local mesh refinement procedure permitting the singularities to be captured economically and accurate results to be obtained with relatively few meshpoints.

RESUME :

On s'intéresse à des écoulements bidimensionnels stationnaires autour d'un profil modélisés par les Equations d'Euler des fluides parfaits compressibles. Avec ce modèle, la solution présente des singularités telles que points d'arrêt et chocs. Dans ce travail, on présente une méthode en éléments finis triangulaires avec raffinement local automatique du maillage, qui permet de capturer ces singularités avec économie et d'obtenir des résultats précis avec peu de points.

0. INTRODUCTION

The idea of adapting the mesh utilized in a numerical simulation to the solution (or to a crude approximation to it) is undoubtedly as old as the notion of discretization itself. A preliminary calculation is made, using an initial mesh, and an adapted mesh is then constructed as a "perturbation" of the initial mesh. Two types of "perturbations" can be considered - the two types are seldomly used at the same time.

1) moving the meshpoints without modifying the topology or total number of them (see {1}, {3}, {4}, {8}, {9}, {10}, {11}, {12}, {15}, {19}, {21}, for example).

2) adding additional nodes (or constructing subgrids)(see{5}, {7}, {22}, for example).
The first approach is attractive because it preserves the topological regularity of finite-difference meshes and also because it permits to cheaply fit discontinuities.
The second approach has recently regained interest, despite its necessarily more complicated implementation, mainly because it is somewhat related to the currently popular multigrid technique (see {6}, {13}, {16}, {18} for example).

In this report we are interested in the second approach in a finite-element context. The advantage of finite-elements resides principally in the generality of the representation of the geometry. In particular, keeping the initial nodes fixed, a local mesh-refinement can be made with no change in the solution method, that is, problems related to patching grids and subgrids or storage problems are automatically solved by the finite-element methodology.
A numerical simulation in which the Euler Equations are used can be an excellent test case for a local mesh refinement method for the following reasons :

- At present, simulations utilizing this model are still very onerous in terms of C P U time per degree of freedom, and it can be of crucial importance to optimize the locations as well as the total number of mesh points.

- The truly interesting results are located on a relatively small part of the computational domain : basically on the airfoil of an airplane wing.

- For industrial applications, the definition of geometries requires a large number of points located on the skin of airfoils.

- The flow contains local singularities such as :

  - shocks (discontinuities of dimension n-1)
  - stagnation points (discontinuities of derivatives, of dimension n-2)
  - slip surfaces, wakes.

Several authors have already investigated the possible use of local mesh refinement for the Euler Equations in a finite-difference context :
- W.J. USAB,Jr and E. M. MURMAN ({20}) associate this idea with a multigrid solution method, but are not interested in the automatic construction of mesh refinement zones.
- Studies of similar nature are announced by M. BERGER ({4}).

Regarding Finite-Element methods, the technique of mesh refinement is still at an early stage for the solution of the Euler Equations (see {14 }).

The present report is organized as follows. We first describe the numerical approximation of the mathematical problem. Then, for a given mesh, we explain the subgridding procedure, the construction of the new mesh and the implementation in the computer program. Then three different local mesh refinements are detailed. One criterion is purely geometrical and is based uniquely on the fact that a good solution is required in the vicinity of the airfoil. A second criterion is based on an estimate of the truncation error. The third criterion is based on the entropy variation, a physical quantity that is very important in the applications.

1. THE APPROXIMATION. THE RICHTMYER SOLVER

Consider the two-dimensional Euler Equations :

$$W_t + [F(w)]_x + [G(w)]_y = 0 \quad \text{in } D$$

\+ Boundary and initial conditions

$$\text{where } W = \begin{Bmatrix} \rho \\ \rho u \\ \rho v \\ \rho E \end{Bmatrix} \; ; \; F(W) = \begin{Bmatrix} \rho u \\ \rho u^2 + p \\ \rho uv \\ (\rho E + p)u \end{Bmatrix} \; ; \; G(W) = \begin{Bmatrix} \rho v \\ \rho u \\ \rho v^2 + p \\ (\rho E + p)v \end{Bmatrix}$$

$$\text{and} \quad E = \frac{1}{2}(u^2 + v^2) + e$$

$$p = (\gamma - 1)\rho e \, , \; \gamma = 1.4$$

ρ is the density.

(u,v) are the (x, y) velocity components, E is the total energy by unit mass, p is the pressure.

Also of interest are the enthalpy H, the Mach number M and the pressure coefficient C_p.

For solver an explicit second-order accurate scheme is used with two-dimensional finite elements. This is a two-stage Richtmyer-type scheme with a P_0-approximation in the predictor step and P_1 in the corrector step (see {2}).

Given a triangulation $\mathcal{T}_h$ of D, assumed to be polygonal, define

$$H_h = \{ \varphi \in L^2(D), \varphi \text{ continuous and linear on each triangle } T \text{ of } \mathcal{T}_h \}$$

$$H_{0,h} = \{ \varphi \in L^2(D), \quad \varphi \text{ constant on each triangle } T \text{ of } \mathcal{T}_h \}$$

$$V_h = H_h \cap H^1(D).$$

For every vertex A of $\mathcal{C}_h$, an integration area A is defined as in the figure below

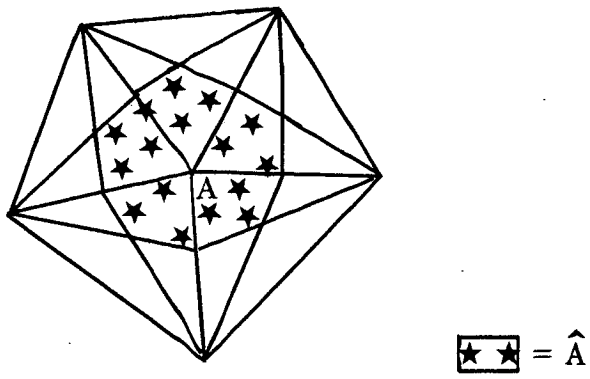

Fig. 1.1 $\hat{A}$ integration area about a vertex of the triangulation.

Let $S_0 = \{ \varphi \in L^2(D), \quad \varphi_{|\hat{A}}$ is constant, for every vertex A of the triangulation $\mathcal{C}_h \}$

The projection operator from H_h onto S_0 is denoted by the symbol S_0.

With this notation, the predictor - corrector sequence is defined as follows :

Step 1 ; Predictor :

$$\begin{cases} \forall T \in \mathcal{C}_h \text{ , and for } k = 1, 2, \ldots 4 \text{ , } \tilde{W}_k \in H^4_{0,h} \\ \\ \tilde{W}_k(T) = \dfrac{1}{\text{area}(T)} \left\{ \iint_T W_k^n \, dxdy \right. \\ \\ \qquad \left. - \alpha \Delta t \int_{\partial T} [F_k(W^n) n_x + G_k(W^n) n_y] \, d\sigma \right\} \end{cases}$$

Step 2 ; Corrector :

$$\begin{cases} W^{n+1} \in (V_h)^4, \text{ and } \forall \phi \in (V_h)^4, \ \forall k = 1, 2, \ldots 4, \\ \iint_D \mathcal{S}_o \left[\frac{W_k^{n+1} - W_k^n}{\Delta t}\right] \mathcal{S}_o \phi_k \, dxdy = & (1) \\ \iint_D^* \{\beta_1 [F_k(W^n) \frac{\partial \phi k}{\partial x} + G_k(W^n) \frac{\partial \phi k}{\partial y}] & (2) \\ + \beta_2 [F_k(\tilde{W}) \frac{\partial \phi k}{\partial x} + G_k(\tilde{W}) \frac{\partial \phi k}{\partial y}]\} \, dxdy & (3) \\ - \int_{\partial D}^* \phi_k [F_k(\bar{W}) n_x + G_k(\bar{W}) n_y] \, d\sigma & (4) \end{cases}$$

$$+ \chi \iint_D f(W^n) \langle \text{grad } W_k^n, \text{ grad } \phi_k \rangle \, dxdy \quad (5)$$

with

$$\alpha = 1 + \frac{\sqrt{5}}{2}, \quad \beta_1 = \frac{2\alpha - 1}{2\alpha}, \quad \beta_2 = \frac{1}{2\alpha}$$

Expression (4) permits us to introduce the physical boundary condition, $\bar{W}$ is a function of W^n and of the nature of the boundary.

Expression (5) is an artificial viscosity term.

2. LOCAL MESH REFINEMENT PROCEDURE

We intend to introduce in the triangulation a preferably small number of additional mesh points. The introduction of the new mesh point is decided automatically by performing a test on every element that relies on one of the criteria defined further. We proceed in the following way :

2.1 First sub-gridding A sweep on the triangulation permits us to switch from global numbering to local numbering of the vertices according to conventional rules dealing with the orientation of each triangle. The subgridding is performed by two topological transformations :

1 - introduction of additional points,

2 - section of some triangles and construction of the new triangulation.

In doing this, a pointer indicating, for every triangle whether it needs to be cut into 4 sub-triangles is assumed to be defined, according to the criterion employed. It remains to construct a finite-element triangulation containing :

1 - The sub-triangles coming from the triangles divided into 4,

2 - triangles identical to those of the initial mesh,

3 - triangles cut in 2, 3 or 4, permitting to patch triangles of type 1 to triangles of type 2: for example, (see Fig. 2.1), if triangle T is the only one to be divided into 4, then it is sufficient to divide into 2 its 3 neighbors to obtain a finite-element triangulation.

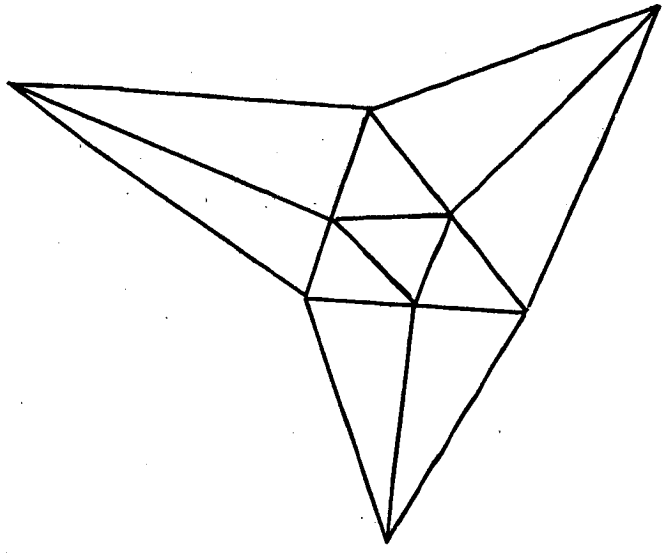

Fig. 2.1 Section of an isolated interior triangle.

Finally, for a triangle T of the initial triangulation 3 cases can occur :

1 According to the criterion, T must be divided into 4 and therefore it is actually cut into 4.

2 T has n neighbors divided into 4, then T is divided into n + 1 subtriangles (see Fig. 2.2).

3 T has no neighbor that is divided and remains unchanged.

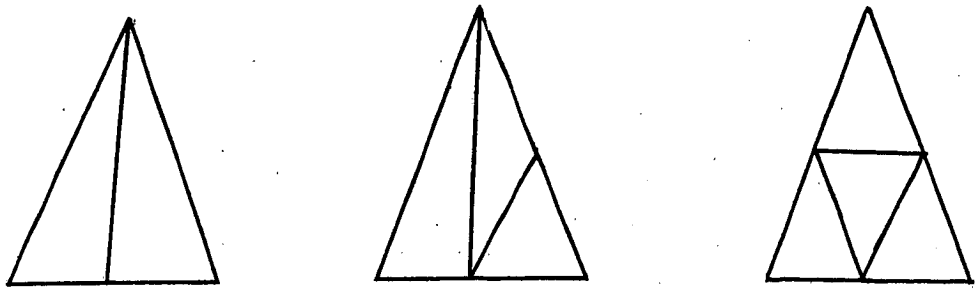

Fig. 2.2 Various ways of dividing a triangle T of $\mathcal{T}_h$.

Clearly, the regularity of the mesh can be degraded by this procedure, in particular, if highly obtuse angles are introduced. Also a good solution accuracy is required on the airfoil. These two remarks leads naturally to introduce the following steps 2.2 and 2.3.

2.2 The "Cosmetic step" By several sweeps on all the triangles and until disappearance of this situation, every triangle divided into 3 is cut into 4, by the adjunction of the midpoint of the unused side. In addition, triangles having 2 vertices on the airfoil and that would normally be divided into 2, are actually divided into 4.

2.3 Projection of the new boundary points The points along the curvilinear boundary are positioned by the following rule : between 2 existant points A and B, a point C is introduced on the airfoil such that $\widehat{CA} = \widehat{CB}$ (see Fig.2.3).

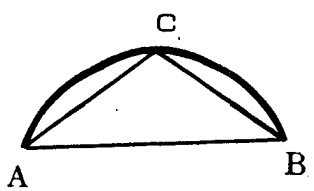

Fif. 2.3 Adjustement of the airfoil definition on a curvilinear portion $\widehat{AB}$.

2.4 Reorganization At the end of the preceding step, the flow-variables at each new point are set equal to the mean of the corresponding flow-variables at the end-points of the segment. Then the complete topological definition of the mesh is reorganized.

3. COMPLETE ALGORITHM

Once the new triangulation is obtained, at the end of step 2, the Euler Equations are again solved by the method detailed in 1. The whole procedure is repeated a number of times prescribed in advance. The algorithm is summarized in the following flow-chart :

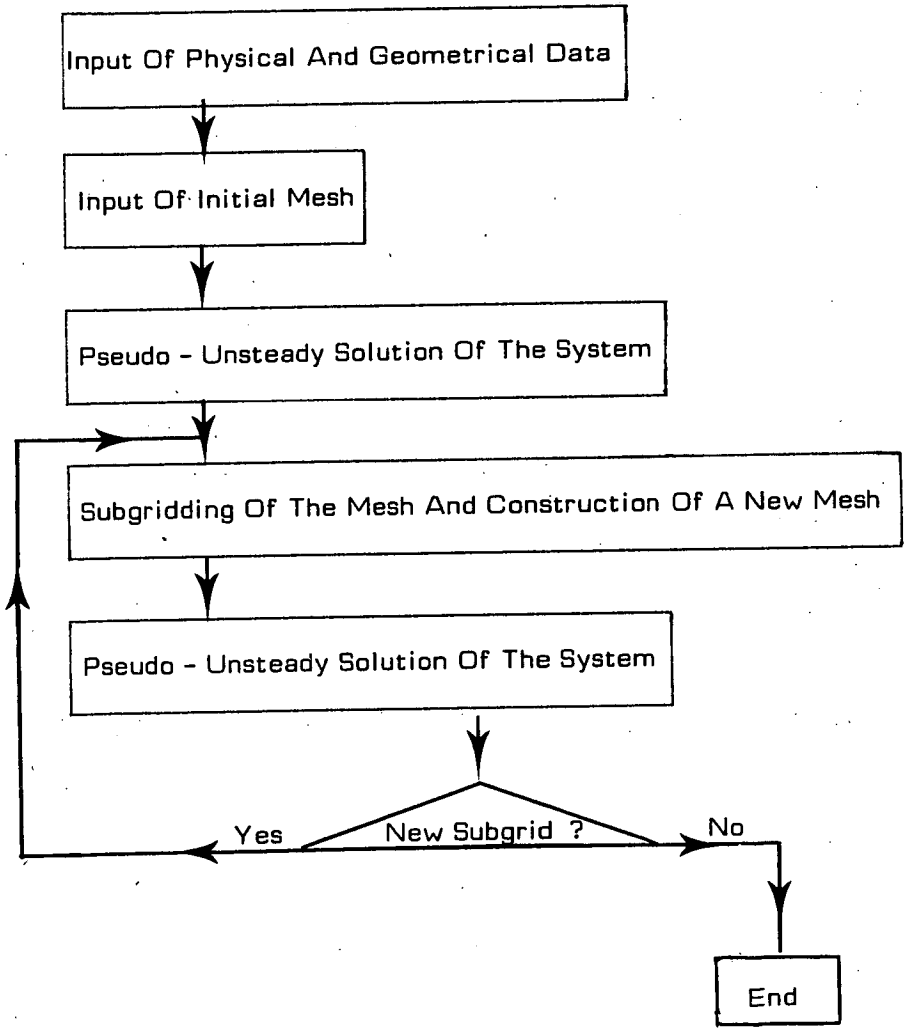

4. CRITERIA APPLIED FOR MESH REFINEMENT

4.1 Geometrical test

The principal interest of the finite-element method relies on the possibility of performing local mesh refinements with simplicity. However these must not imply degradation of the numerical approximation. In theory, P_1 - elements converge for families of possibly irregular triangulations. We intend to verify this point of theory and, more precisely, to investigate what happens when a shock is present. The method that is employed consist in systematically dividing into 4 all the triangles with at least one vertex on the skin of the airfoil. This procedure being followed by the "Cosmetic" step and then by the possible projection of new boundary points.

4.2 Test on the error estimate

We now search for a criterion that would, first diminish the error in the numerical solution of the Euler Equations and second avoid to introduce unnecessary points and still emphasize the shock zone. We recall that the final objective is to solve the steady Euler Equations

$$(4.1) \quad \begin{cases} [F(W)]_x + [G(W)]_y = 0 \\ + \text{ Boundary Conditions} \end{cases}$$

from the calculation of the time dependent solution.

$$(4.2) \quad \begin{cases} \hat{W} = \lim_{t \to \infty} W_t \,, \; W_t \text{ solution of} \\ \dfrac{\partial W_t}{\partial t} + [F(W_t)]_x + [G(W_t)]_y = 0 \\ + \text{ Boundary and initial Conditions} \end{cases}$$

If the above system were solved exactly, the following equation would be satisfied at every node (x, y) of the integration domain.

$$(4.3) \qquad E(x, y) \equiv [F(\hat{W})]_x + [G(\hat{W})]_y = 0$$

The function $\hat{W}(x, y)$ is calculated at every point of the integration domain D by means of P_1 interpolation. But the P_1 finite-element approximation contrasting with finite-differencing produces a solution that is determined over the entire integration domain and not uniquely at the nodes of the mesh. A fundamental difference between the obtained discrete solution $\hat{W}_d$ and the exact solution W is that the discrete solution does not satisfy the equations and, for example, we have in general :

$$(4.4) \qquad E_d(x, y) \equiv [F(\hat{W}_d)]_x + [G(\hat{W}_d)]_y \neq 0$$

When F and G are linear functions $E_d(x, y)$ is piecewise constant on the triangles and it is easy to compare it to 0. In the case where F and G are not linear, one can replace $F(\hat{W}_d)$ and $G(\hat{W}_d)$ by the linear interpolants. $F_1(\hat{W}_d)$ and $G_1(\hat{W}_d)$ so that :

$$(4.5) \qquad E_1(x, y) \equiv [F_1(\hat{W}_d)]_x + [G_1(\hat{W}_d)]_y$$

is again constant on every triangle. It is conceivable that this quantity truly represents the discretization error. In fact a test based on this quantity can be interpreted as the comparison of two approximations of the Euler Equations, one centered at the nodes (Richtmyer scheme) and the other centered on the triangles (Staggered approximation).

The method is as follows :
- Is divided into 4 every triangle T_0 of the triangulation $\mathcal{T}_h$ for which E_1 (averaged over the triangle T_0) is "too large" in the sense that, for one component $(E_1)_i$ at least.

$$(E_1)_i \geq C\ (E_1\ \max)_i \tag{4.6}$$

in which $(E_1\ \max)_i = \max_{T \in \mathcal{T}_h} (E_1)_i$.

The value of the parameter C is obsviously problem-dependent.

4.3 Test on the numerical entropy production

An alternate measure of the discretization error consists in evaluating how closely the equation :

$$u \frac{\partial s}{\partial x} + v \frac{\partial s}{\partial y} = 0 \tag{4.7}$$

in which $s = \frac{p}{\rho^\gamma}$ is the entropy,

is satisfied.

Note that (4.7) is only true when the flow is smooth, so that the quantity

$$u \frac{\partial s}{\partial x} + v \frac{\partial s}{\partial y}$$

is expected not to be small, either if the approximation is not accurate enough, or near a singularity. In both cases, it is advantageous to locally refine the mesh. This leads us to define an alternate test for dividing triangles (according to the same rules as previously) in which in the mean :

$$(4.8) \qquad u\frac{\partial s}{\partial x} + v\frac{\partial s}{\partial y} \geq C \left(u\frac{\partial s}{\partial x} + v\frac{\partial s}{\partial y}\right)_{max}$$

where $$\left(u\frac{\partial s}{\partial x} + v\frac{\partial s}{\partial y}\right)_{max} = \max \left| u\frac{\partial s}{\partial x} + v\frac{\partial s}{\partial y} \right|$$

5. NUMERICAL RESULTS

5.1 Model Problems

5.1.1 Test case N° - 1 of the Stockholm GAMM Workshop (1979)

This case deals with the flow over a 4.2 % thick circular bump at zero incidence in a constant-area channel

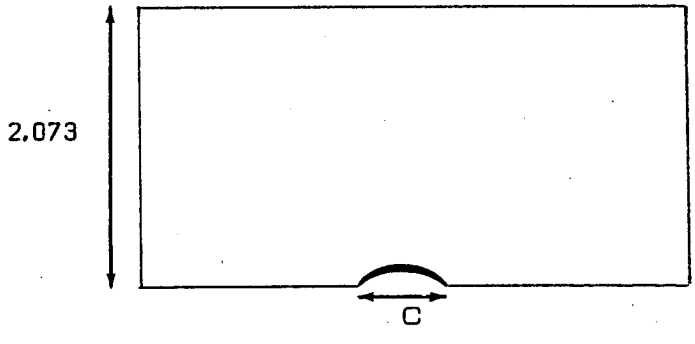

C is the chord. The coarse mesh is made of 23 x 7 = 161 points and of 264 triangles with 11 uniformely-spaced points on the bump. The Mach number is 0.85. With the resolution of the coarse grid [Fig.6.1, 6.3, 6.7, 6.9, 6.11], the shock is not clearly positioned in the Mach contours or in the pressure plots. The compression before the trailing edge is not apparent. The entropy variation is not equal to zero before the shock. As reference, the solution of the same problem as in test case N° 1 but obtained over a finer mesh with 72 x 21 = 1512 grid points, also uniformly-spaced over the bump, is used [Fig. 6.2, 6.5]. In this solution, the shock is well defined, as it can be seen from the Mach contours [Fig. 6.4, 6.6], as well as from the pressure plots [Fig. 6.8]. The discontinuity is more accentuated, the shock is steeper, and away from the shock these curves are smoother. Regarding the entropy deviation [Fig. 6.10], it is closer to the theoretical result since it is approximately 0 before the shock. Note that this calculation was made with the same solver as previously with the coarse mesh, but with a sharper selection of the artificial viscosity coefficient and of the Courant number [see {17}].

5.1.2 A NACA 0012 airfoil flow at no incidence

For a Mach number of 0.72. The initial mesh made of 600 points and of 1080 triangles, with 60 grids points on the airfoil, is also uniform in the x-direction over the airfoil [Fig. 7.1 to 7.7].

5.2 Results for Test-Case N° 1 of the GAMM Workshop

For the three methods, two successive mesh refinements are performed. The artificial viscosity is the same [Von Neumann - Richtmyer] and its coefficient χ is 0.8. As initial solution, a uniform flow is enforced. To test the convergence of the solver, a tolerance on the residual is taken to be 10^{-4}. In the last two methods, the constant C has the value 0.05.

Table 1 below permits us to compare the efficiency of the various methods.

Test-case	Coarse mesh	Fine mesh	Geometrical test	Test on the error estimate	Test on entropy
N° of grid points	161	1512	411	294	367
Total CPU time (CII, HB 68)	20'	480'	240' *	51'	67'

Table 1 : Numerical results of Test-Case N° 1 of the GAMM Workshop.

5.2.1 Geometrical test

Because the mesh refinement (Fig. 6.13, 6.15) is here very localized, the Mach contours (Fig. 6.14, 6.16) do not show a very sensible improvement at first sight. Nevertheless we observe a much thinner shock in the area that is refined. So that the shock is better captured there. This is confirmed by the pressure distribution (Fig. 6.17) that indicates a clear improvement realized by the calculation on the refined mesh.
In particular, the stagnation points are better resolved and the shock is sharper.
In addition, the comparison of these results to those obtained over the fine mesh (Fig. 6.2, 6.4, 6.5, 6.6, 6.8, 6.10) indicates that the shock is correctly located.
Therefore these results demonstrate the capability of the approximation used in these calculations to allow for rather abrupt local mesh refinements.
We would like to obtain a solution accurate everywhere and a sharp shock :
We turn now to mesh refinements better adapted to the solution.

* Here, the evident slow convergence can be explained by the fact that the successive refinements were made not only along the body but also at infinity.

5.2.2 Test on the error-estimate

We note very clear inprovement on the number of the mesh points and the C P U - time compared to the previous results, while the Mach contours and pressure and entropy plots remain very close (Fig. 6.19 to 6.24). We also observe that this improvement realized by this solution over that obtained on the coarse mesh is achieved by the sole addition of mesh points near the leading and trailing edges of the bump. This test does not seem sensitive enough to increase the solution accuracy near the whole shock.

5.2.3 Test on the entropy production

This test defines a mesh made of slightly fewer points than the mesh defined by the geometrical test.Moreover, the location of these points indicates that this test is more selective. It introduces mesh points solely at the leading and trailing edges and near the shock (Fig. 6.25 to 6.30). It follows a very sensible improvement in the Mach contours from which the shock is apparent over a height away from the bump only slightly less then that of the fine mesh calculation. The pressure curves indicate a thinner shock relatively to the previous results, while the gain on the entropy is not uniform along the x-axis. The solution accuracy is globally increased not only at certain y-stations but over the entire domain.

5.3 Results for the NACA 0012 airfoil

The aim of these experiments is the same as for those conducted on Test-Case N° 1 of the GAMM Workshop. Here only local mesh refinement is performed and this, for the three methods. The initial solution is taken to be a solution obtained on the coarse mesh and for which the norm of the residual was only converged to 10^{-2}. No artificial viscosity is employed ($\chi = 0$). The convergence test for the solver remains fixed to the value 10^{-4}. The constant C employed in the last two methods is set to the value 0.05.

5.3.1 Geometrical test

The number of mesh points increases from 600 to 840. For the NACA 0012 airfoil at a Mach number.72, we observe that this test is not restrictive enough (Fig. 7.8 to 7.13). Furthermore, in the absence of artificial viscosity added, oscillations appear. The pressure plots are slightly improved, the stagnation points being a little better resolved, since the pressure coefficient at the leading edge goes from 0.933 to 0.990. The amplitude of the oscillations near the trailing edge is clearly reduced. Regarding the entropy deviation along the body, the improvement is not evident. Negatives values have disappeared but the mean value has increased. Beyond the trailing edge, the entropy produced is twice smaller. The Mach contours are smoothed near the airfoil except for some small oscillations probably due to the fact that the Mach number approches 1.

5.3.2 Test on the error-estimate

The number of mesh pointsincreases from 600 to 678. The results are far better than in the previous method (Fig. 7.14 to 7.20). The oscillations have practically disappeared from the pressure plots. Regarding entropy, negative values have disappeared and the mean value has decreased relatively to the result of the coarse mesh calculation. The entropy contours are in a lesser number near the airfoil. The Mach contours are smoother than in the previous case and the oscillation that used to appear near the airfoil has vanished.

5.3.3 Test on the entropy production

The number of mesh points increases from 600 to 735. The results of this method realize an improvement over those of the previous method but each one to a different degree (Fig. 7.21 to 7.27). The oscillations on the pressure plots have nearly completely disappeared. The entropy mean value has decreased, but oscillations at small negative values appear near the leading edge. The Mach contours are very clearly smoother. The entropy contours are fewer, indicating that the entropy variations are lesser except near the leading edge where small oscillations are still present.

5.4 Conclusion

The results obtained are very encouraging from several view points :

- First, regarding solution accuracy, we note that the scheme performs fairly well even in the case of rather abrupt changes in the geometry. The singularities are well positioned for the examples presented. However the calculations indicate a difficulty dealing with the proper adjustement of the viscosity parameter. To overcome this difficulty, we plan in a future work to utilize a scheme with no artificial viscosity parameter to adjust.

- Finally, regarding efficiency, the improvement appears at two levels : first, the lesser number of mesh points reduces the computational work per iteration; second, the convergence of the scheme is more rapid when a large meshsize is conserved, as in the present case, far from the airfoil. In the future we intend to extend this work and further improve convergence by applying a multigrid methodology.

6. TEST CASE N° 1 OF THE GAMM WORKSHOP

6.1 Model problems

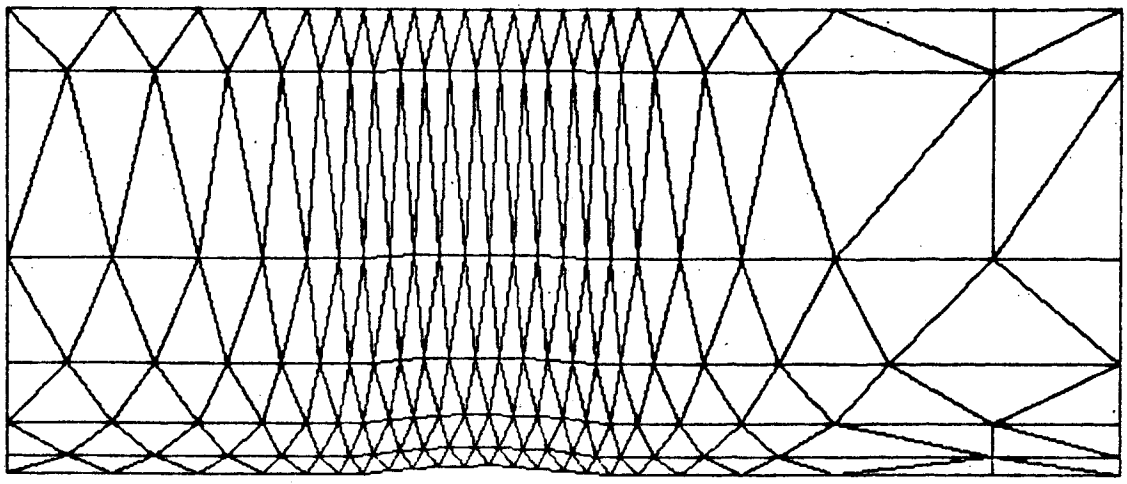

Figure 6.1 Coarse mesh (161 points)

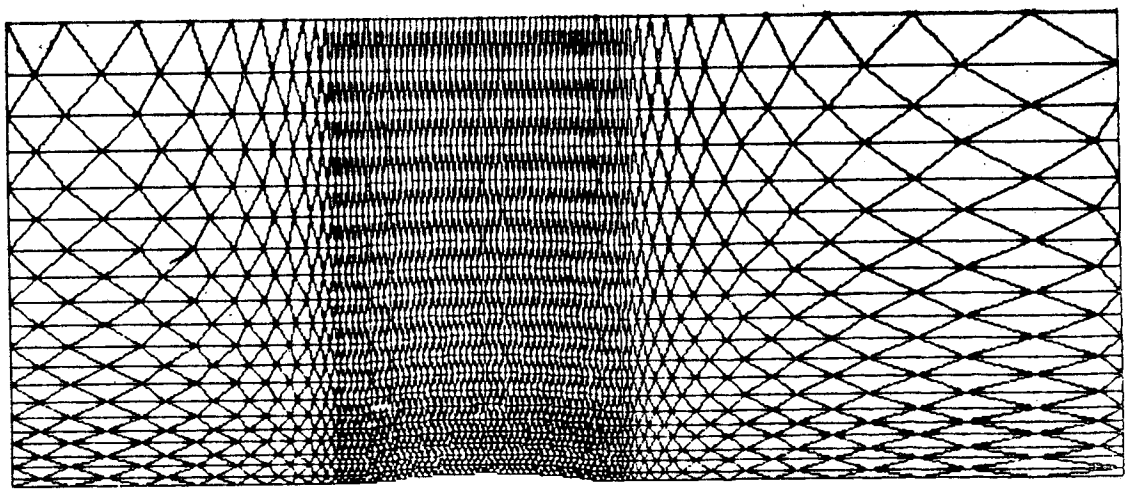

Figure 6.2 Fine mesh (1512 points)

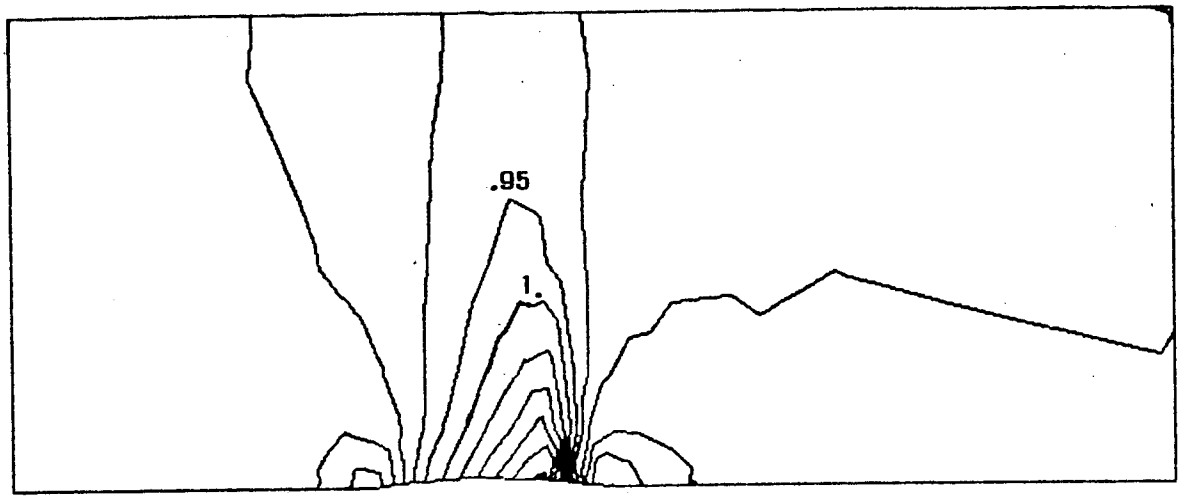

Figure 6.3 Mach contours (coarse mesh calculation)

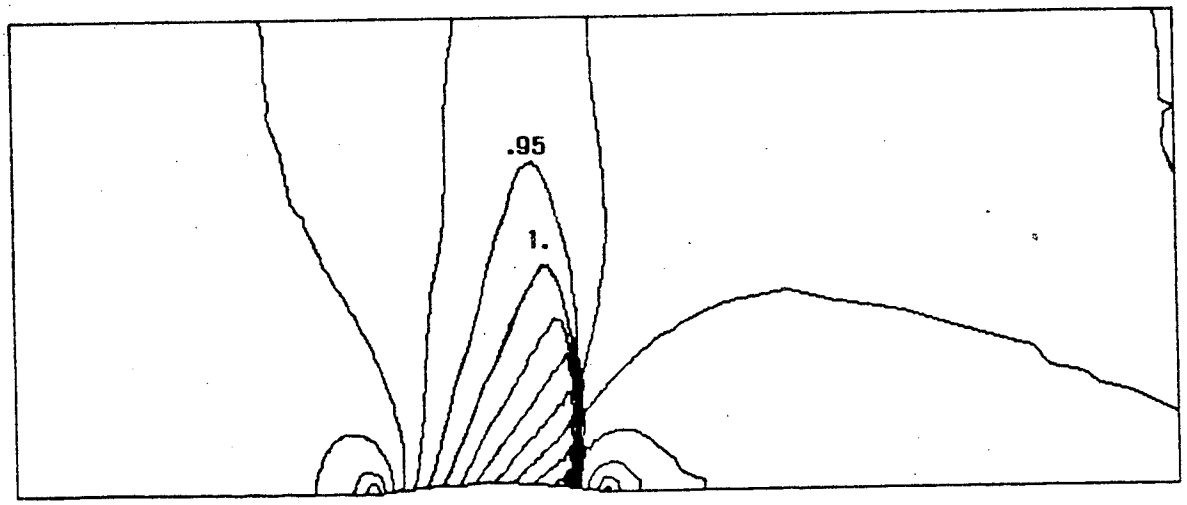

Figure 6.4 Mach contours (fine mesh calculation)

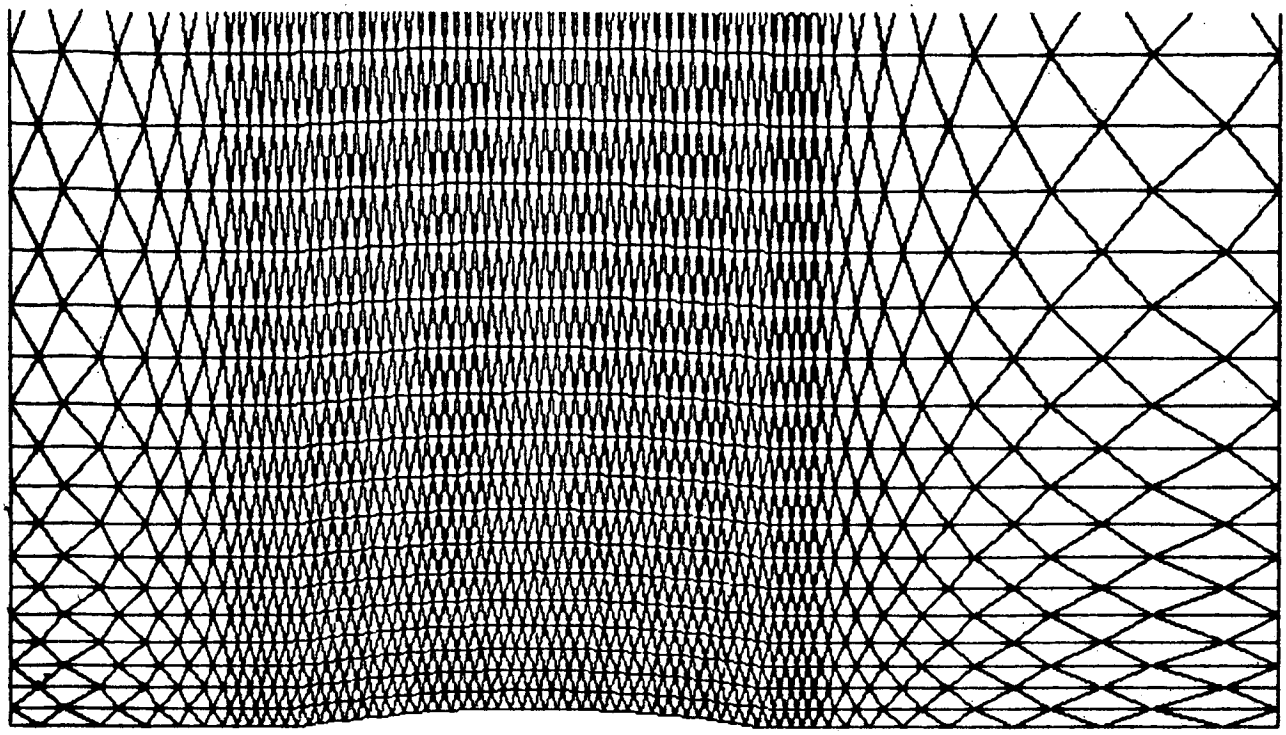

Figure 6.5 Blow-up of the fine mesh

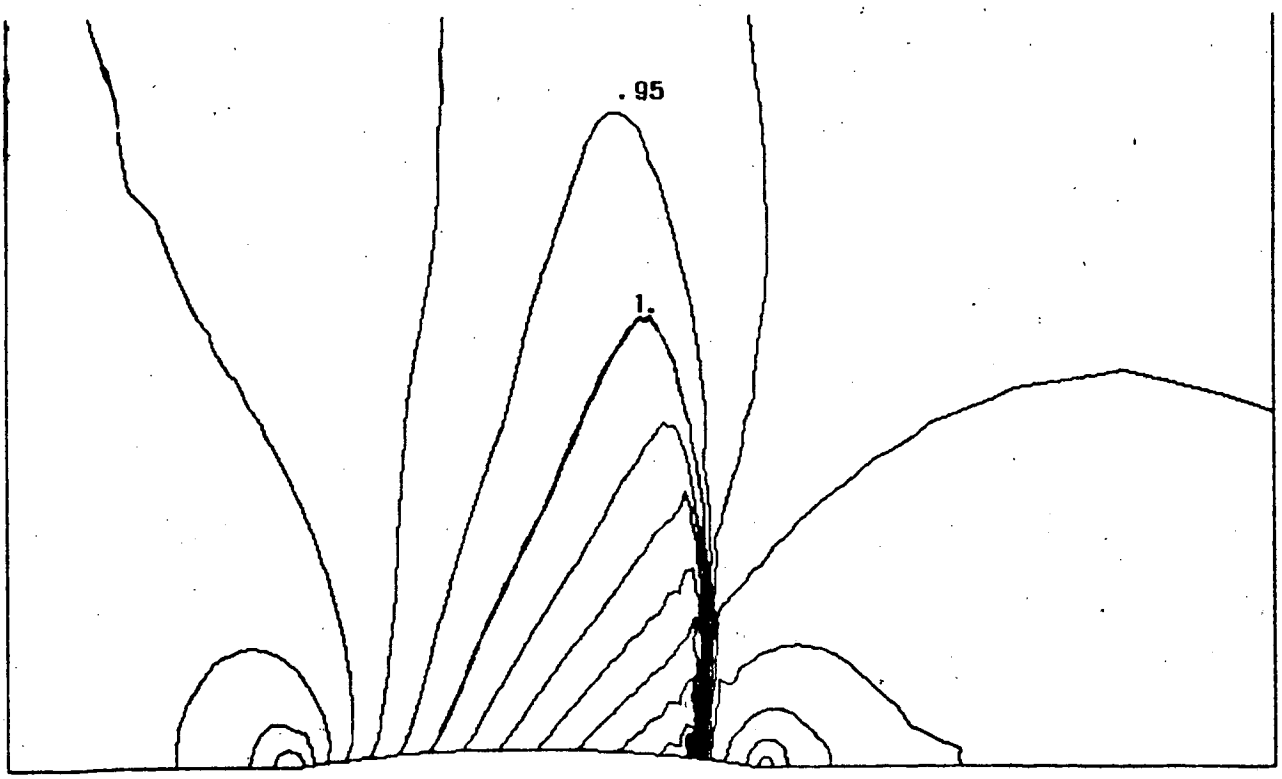

Figure 6.6 Corresponding blow-up of the Mach contours (fine mesh calculation)

MIN : -.2870376E+00 - MAX : 0.7430344E+00

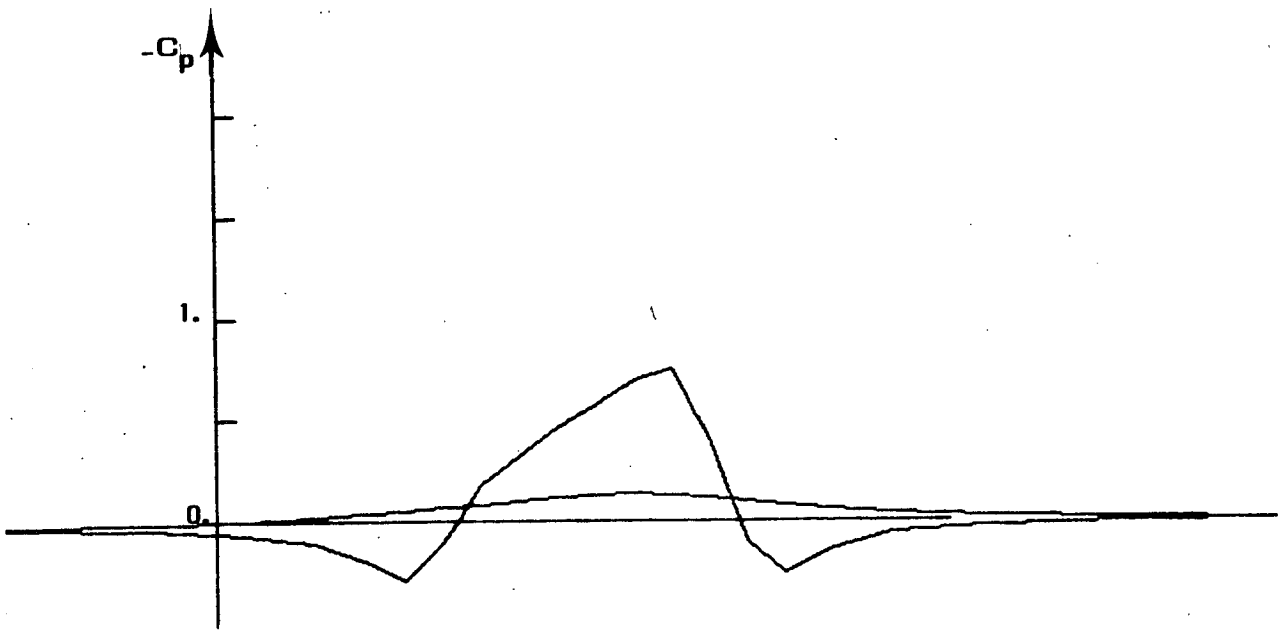

Figure 6.7 Pressure (Coarse mesh calculation)

MIN : -.4385572E+00 - MAX : 0.8605267E+00

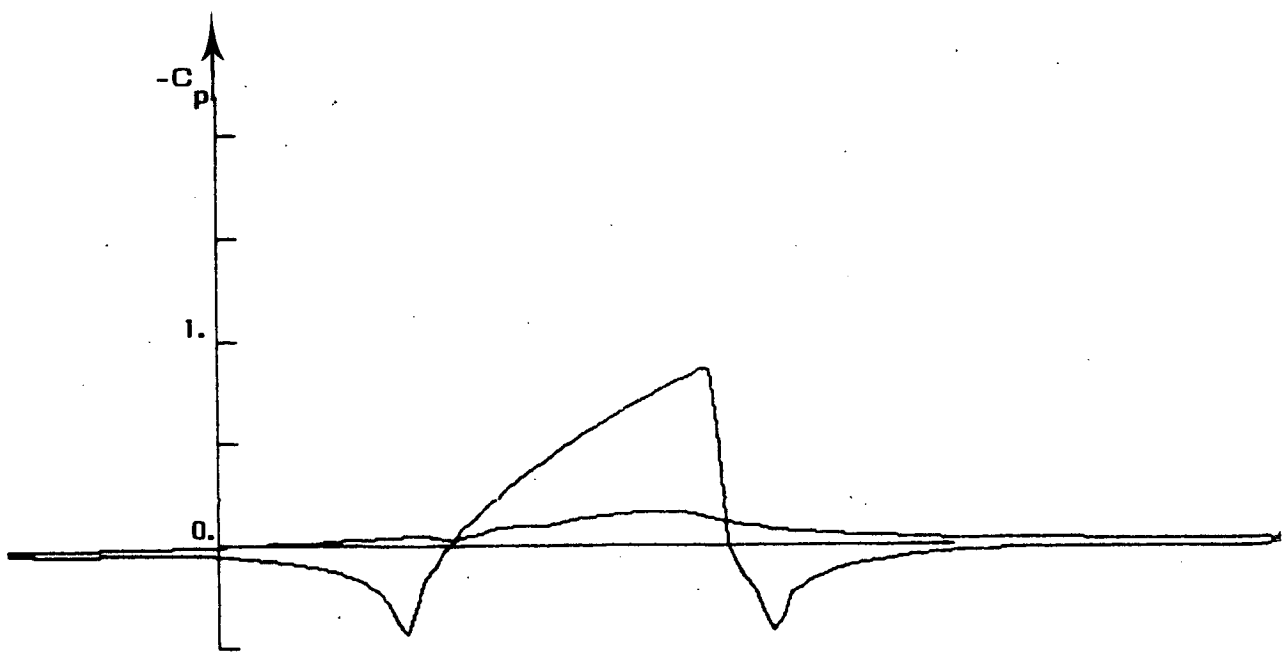

Figure 6.8 Pressure (fine mesh calculation)

MIN : -.1252238E-01 - MAX : 0.1825996E-01

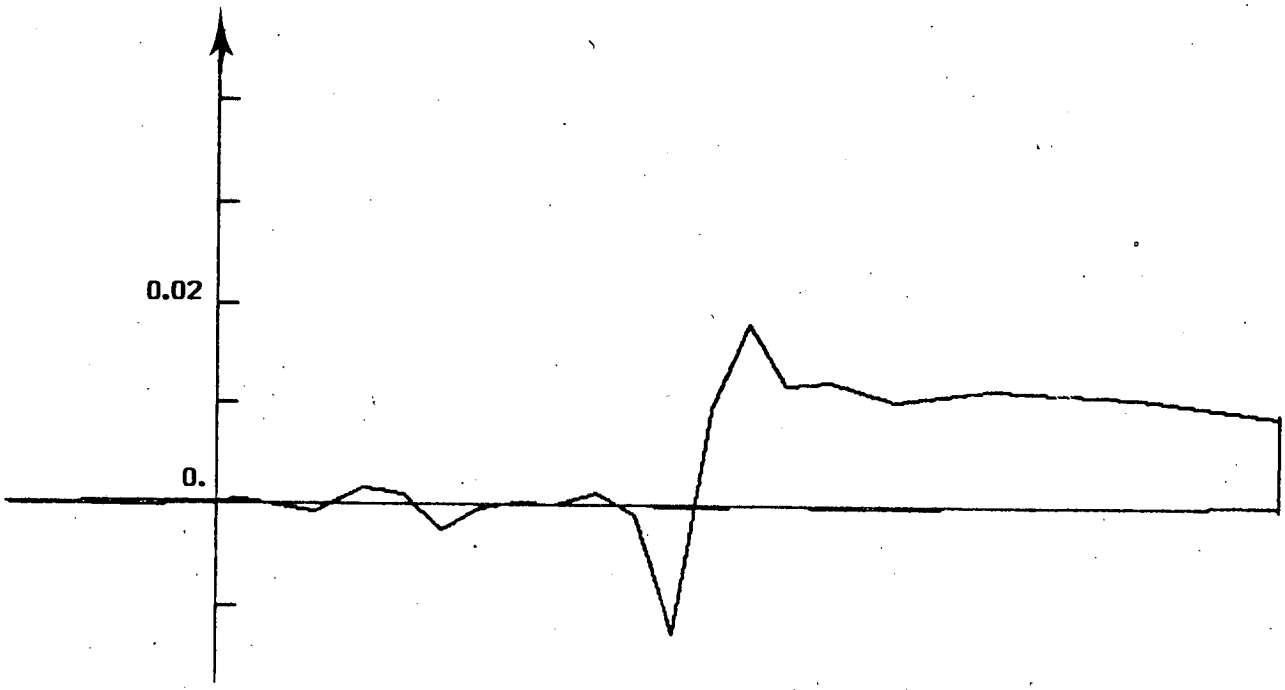

Figure 6.9 Entropy (coarse mesh calculation)

MIN : -.3248958E-03 - MAX : 0.1170418E-01

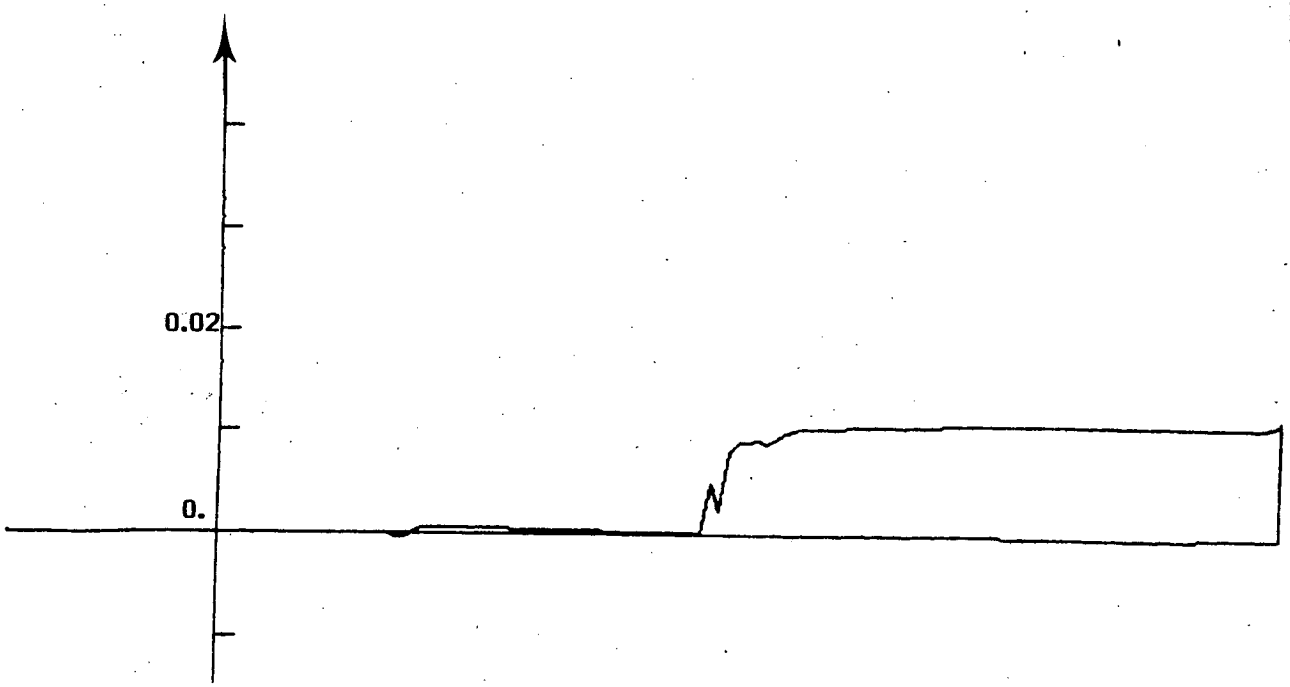

Figure 6.10 Entropy (fine mesh calculation)

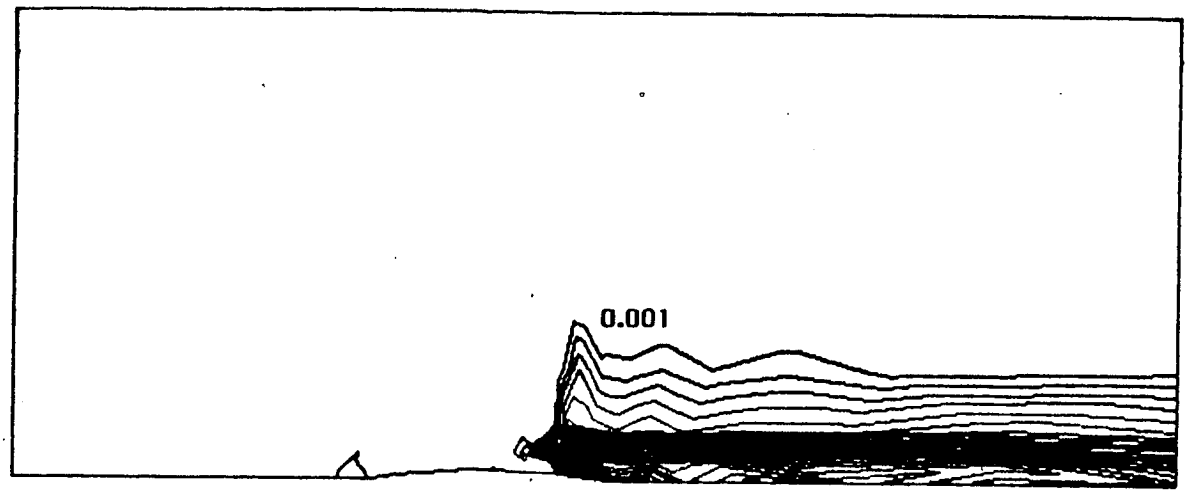

Figure 6.11 Entropy contours (coarse mesh calculation)
(Δs = 0.001)

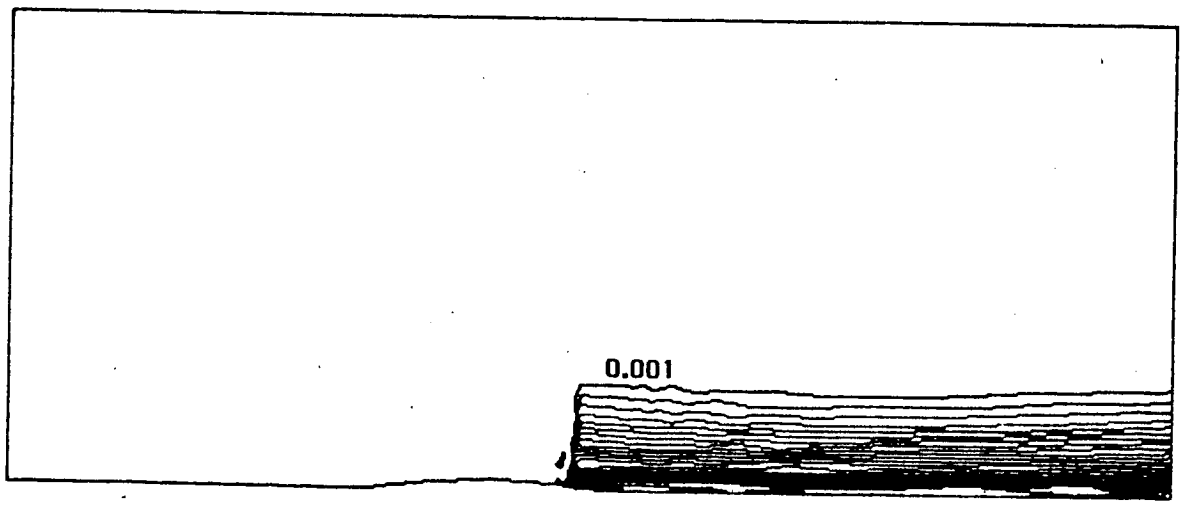

Figure 6.12 Entropy contours (fine mesh calculation)
(Δs = 0.001)

6.2 Results obtained using geometrical test

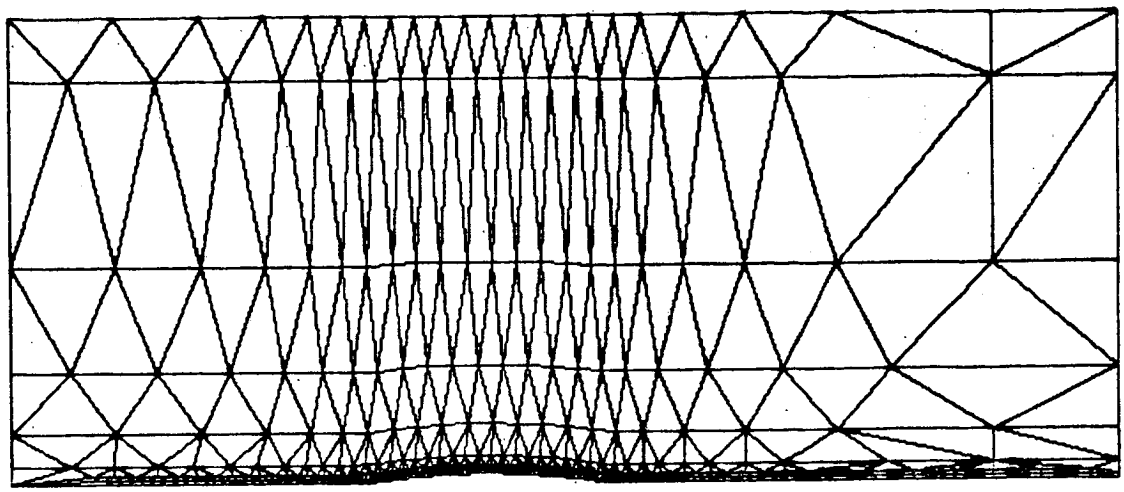

Figure 6.13 Final mesh (411 points)

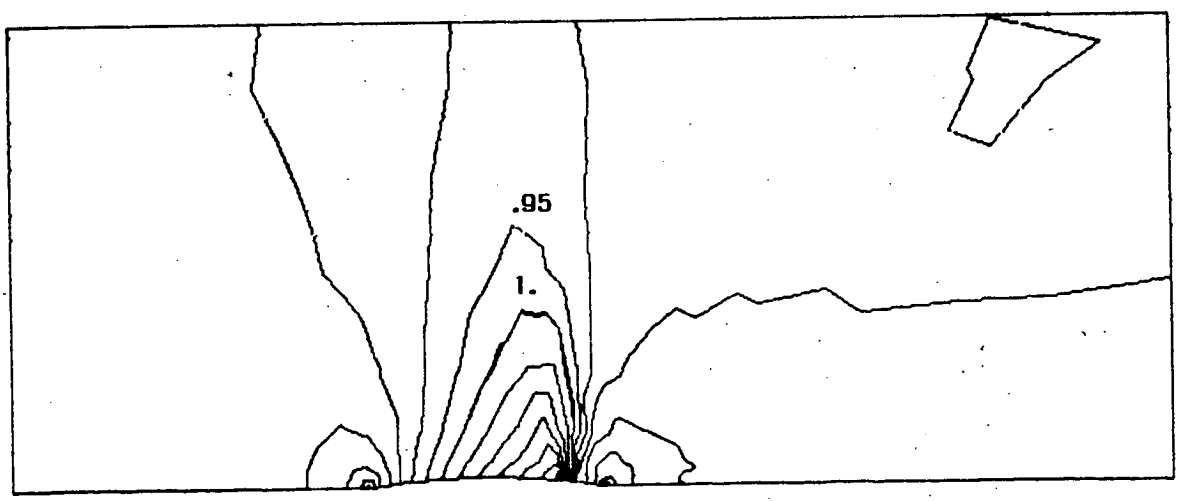

Figure 6.14 Mach contours

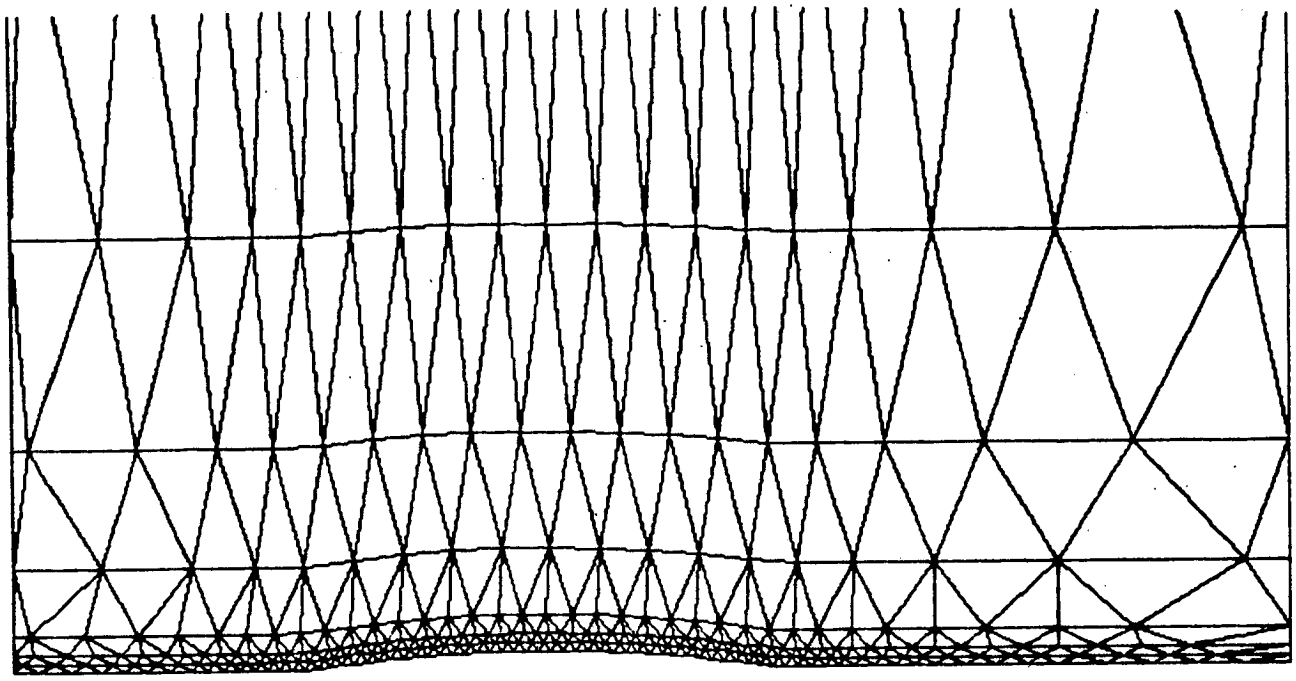

Figure 6.15 Blow-up of the final mesh

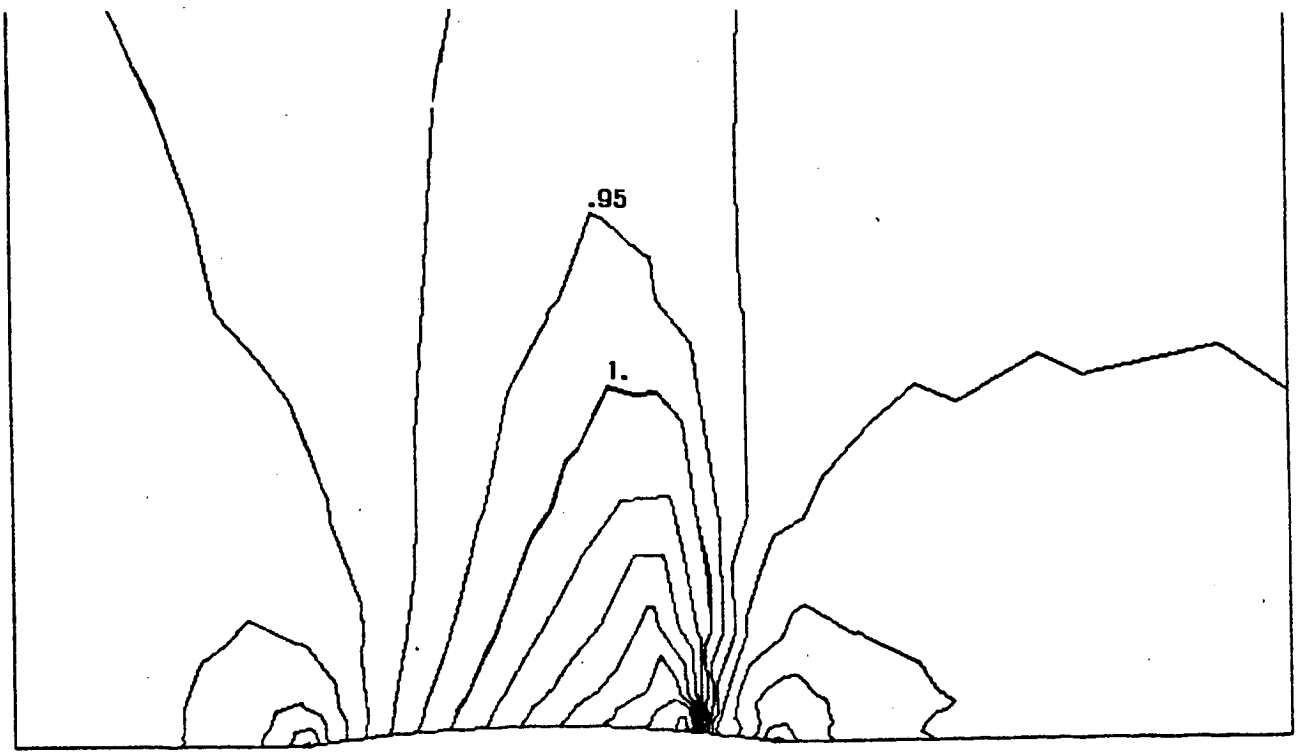

Figure 6.16 Corresponding blow-up of the Mach contours

MIN : -.4397351E+00 - MAX : 0.8334796E+00

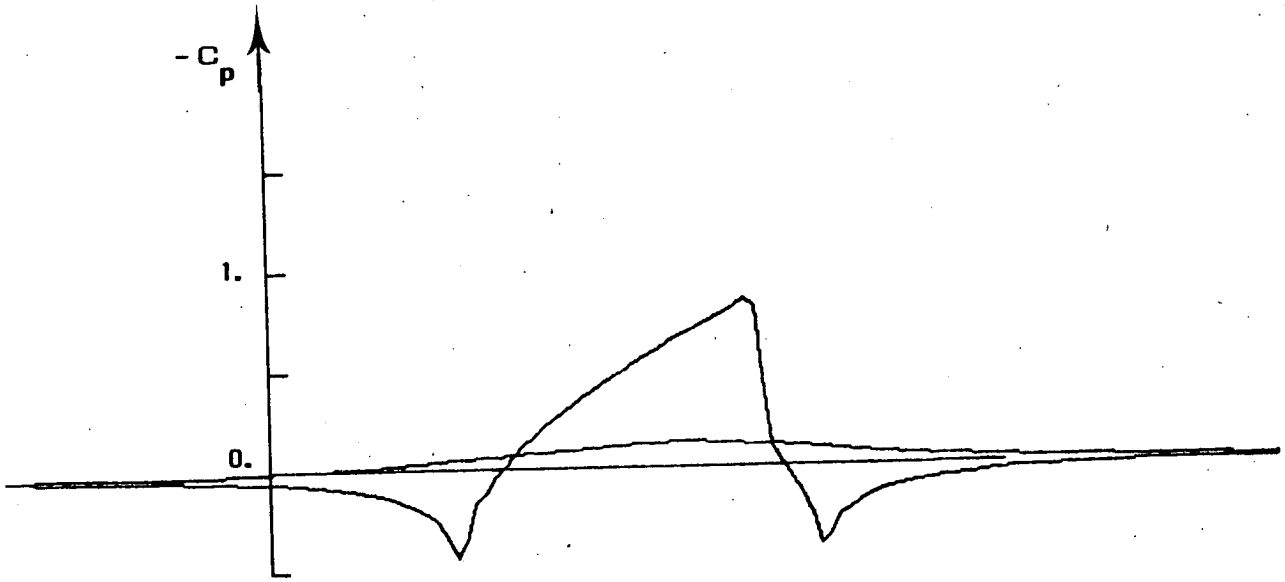

Figure 6.17 Pressure

MIN : -.7101775E-02 - MAX : 0.1172383E-01

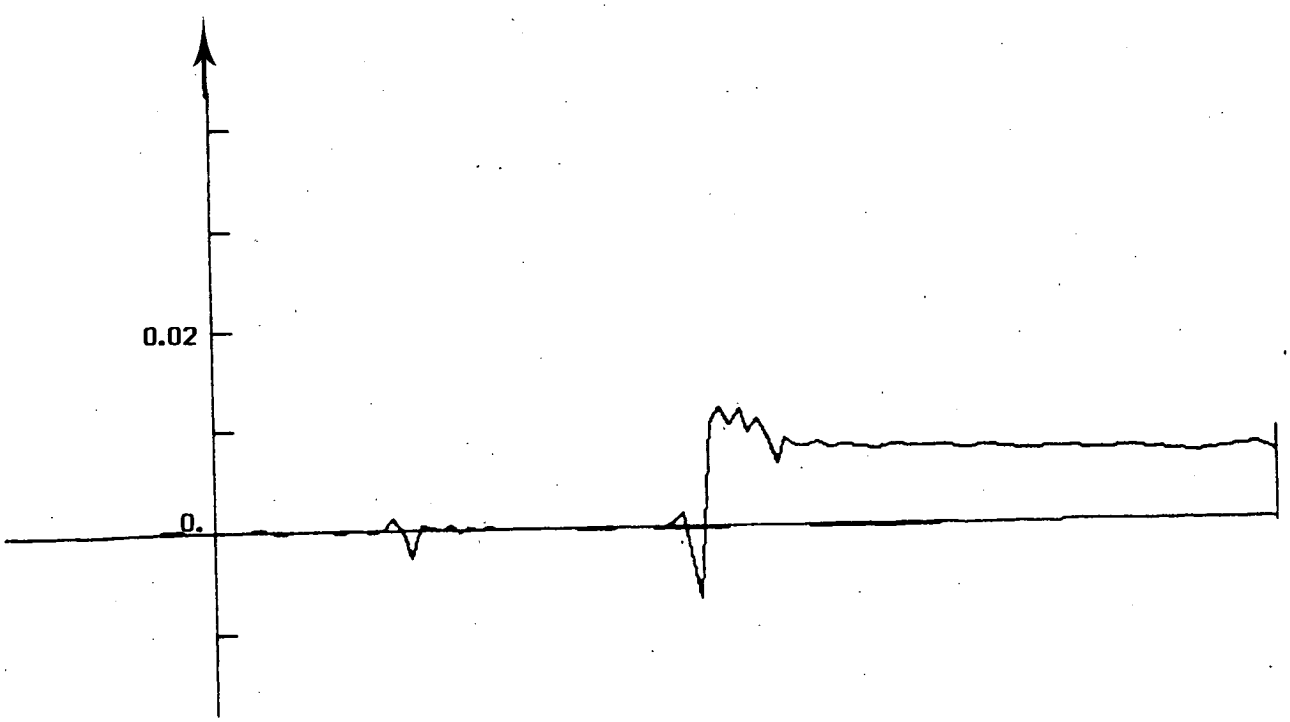

Figure 6.18 Entropy

6.3 Results obtained using the test on the error-estimate

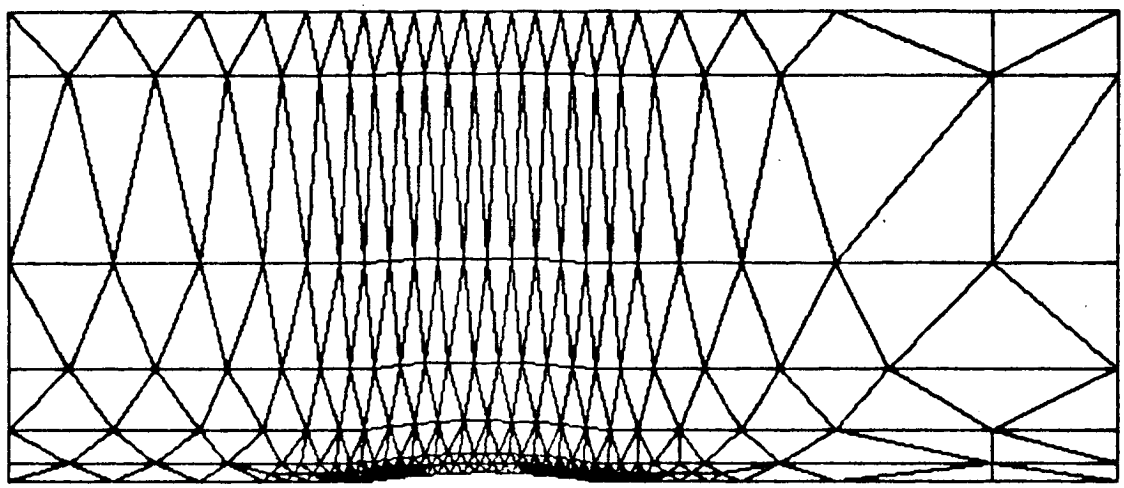

Figure 6.19 Final mesh (294 points)

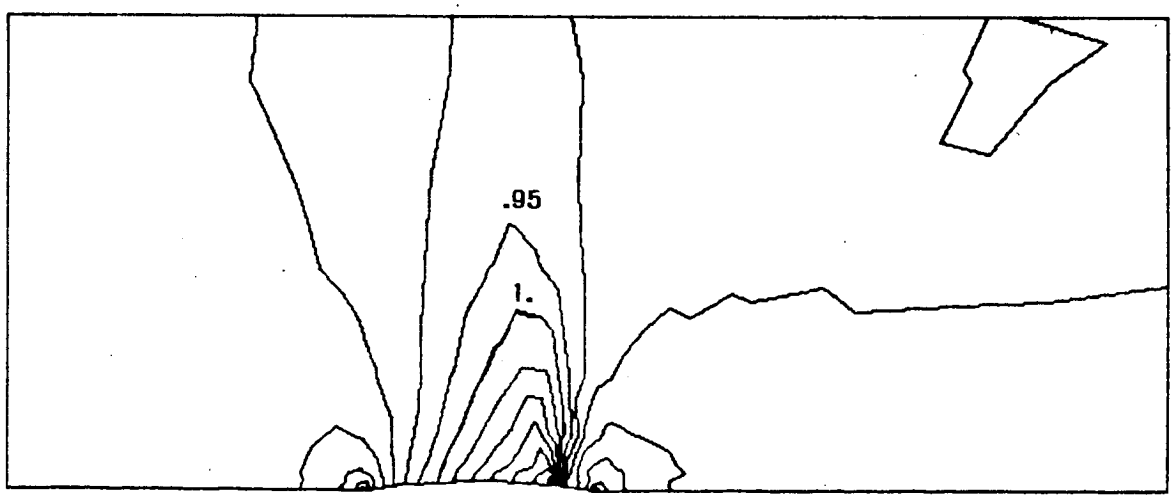

Figure 6.20 Mach contours

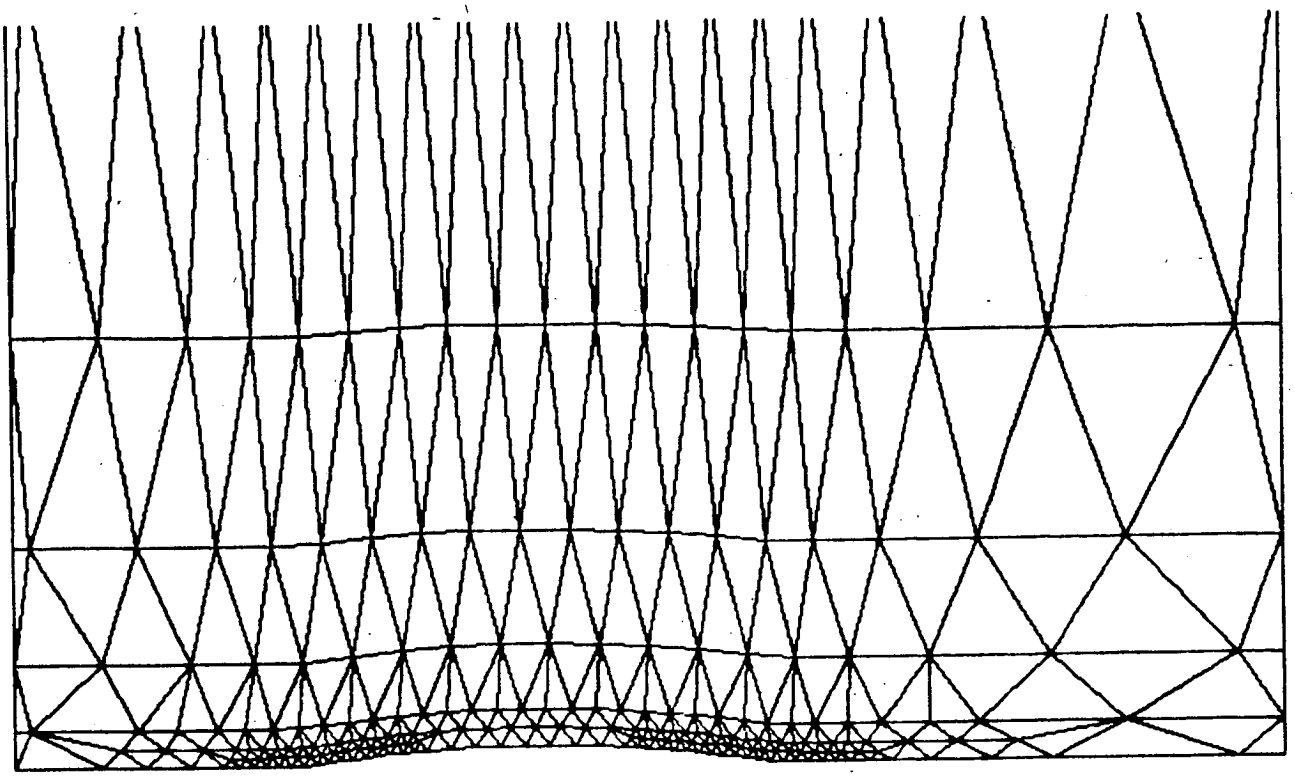

Figure 6.21 Blow-up of the final mesh

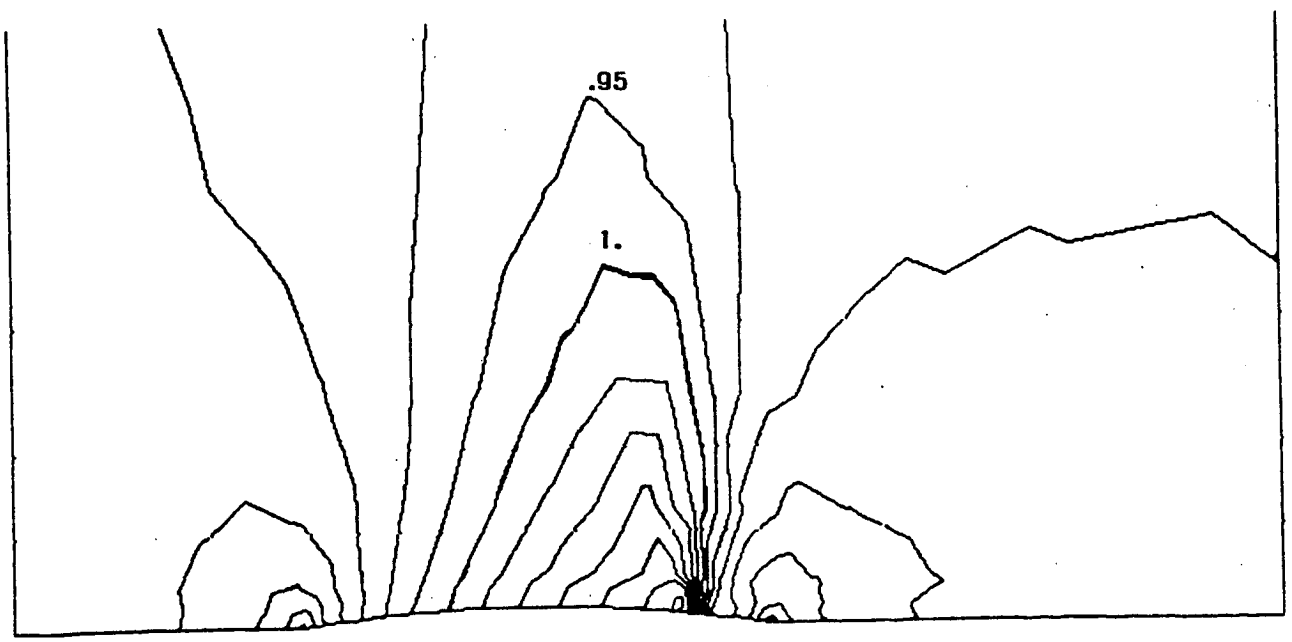

Figure 6.22 Corresponding blow-up of the Mach contours

MIN : -.4391107E+00 - MAX : 0.8316379E+00

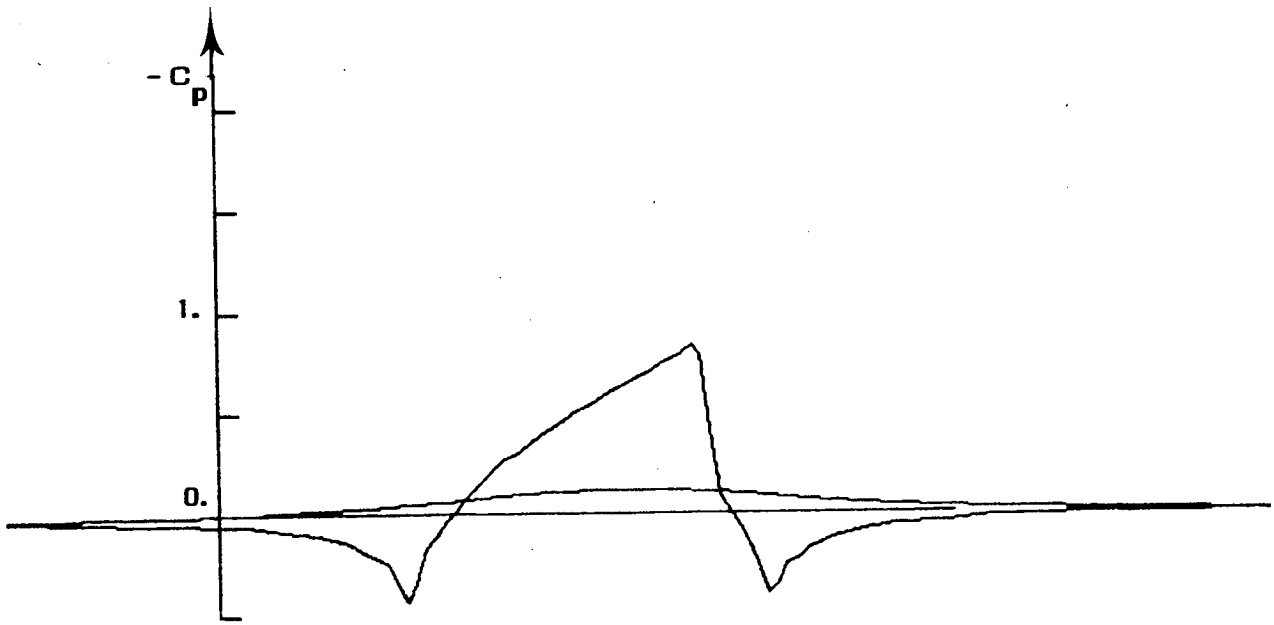

Figure 6.23 Pressure

MIN : -.5577200E-02 - MAX : 0.1248111E-01

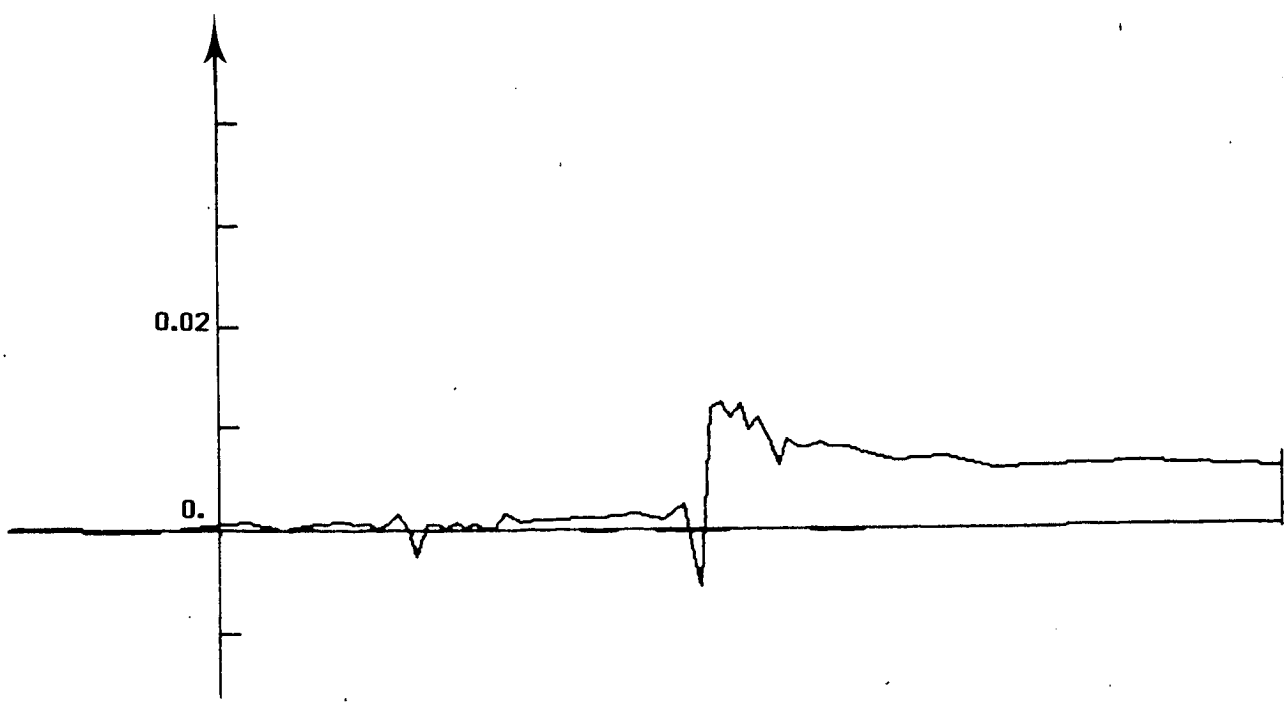

Figure 6.24 Entropy

6.4 Results obtained using the test on entropy

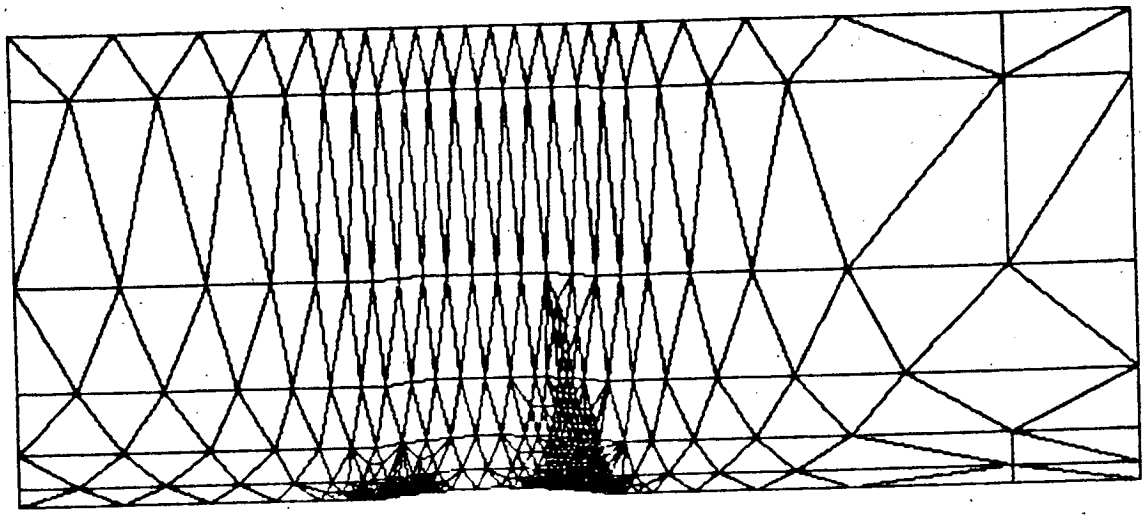

Figure 6.25 Final mesh (367 points)

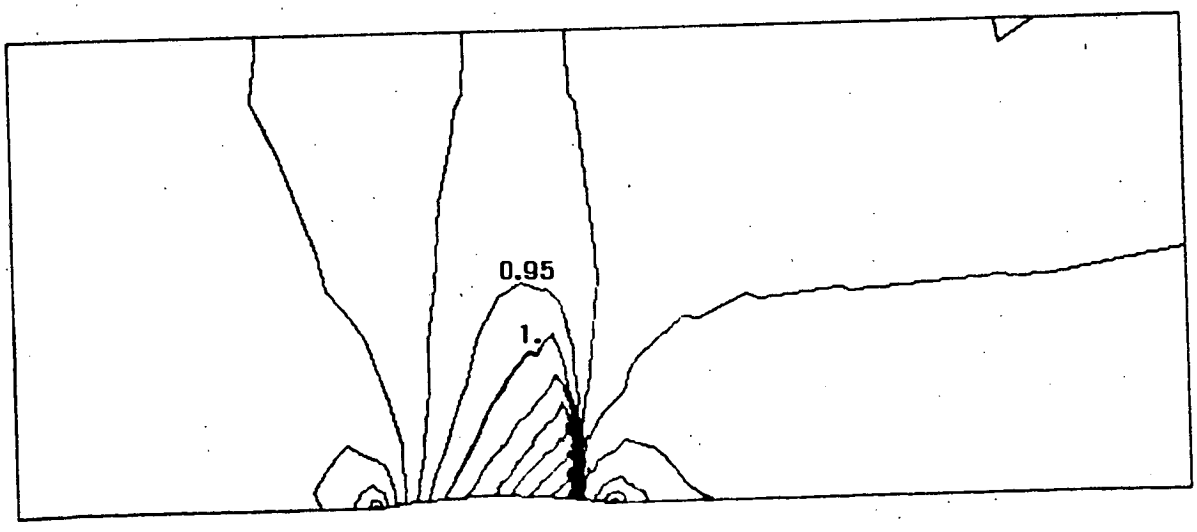

Figure 6.26 Mach contours

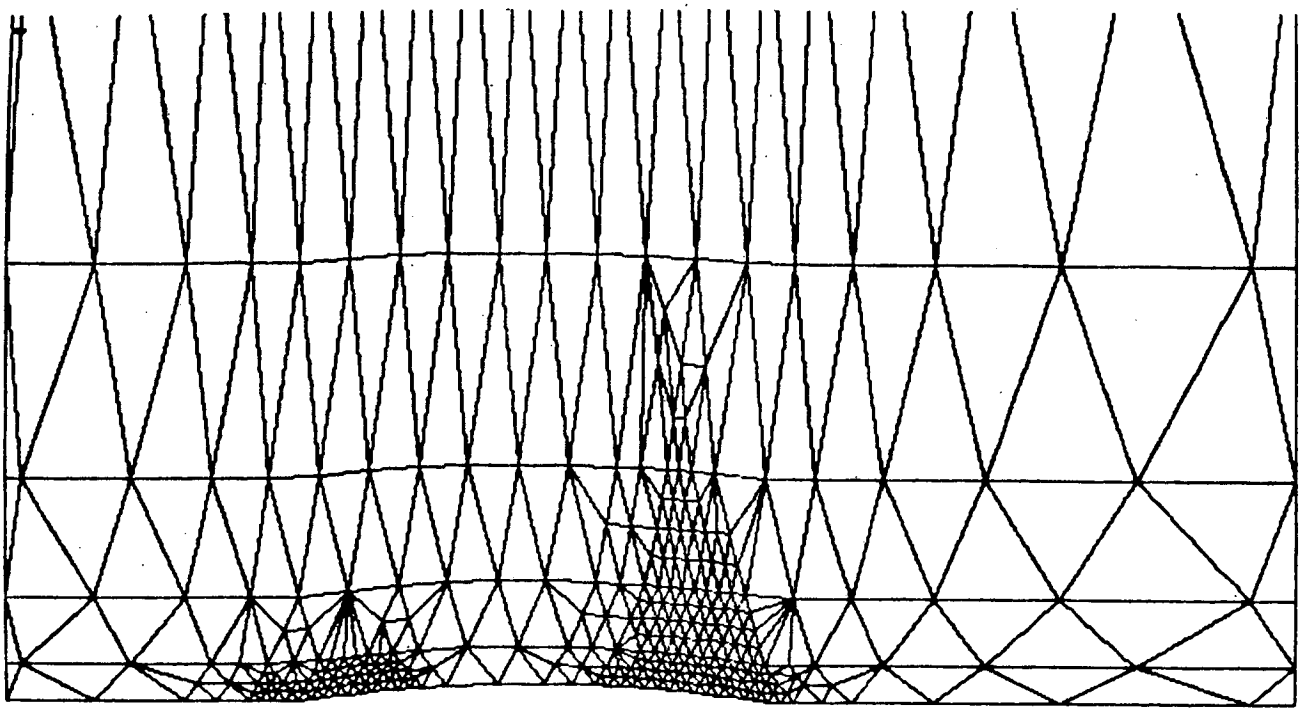

Figure 6.27 Blow-up of the final mesh

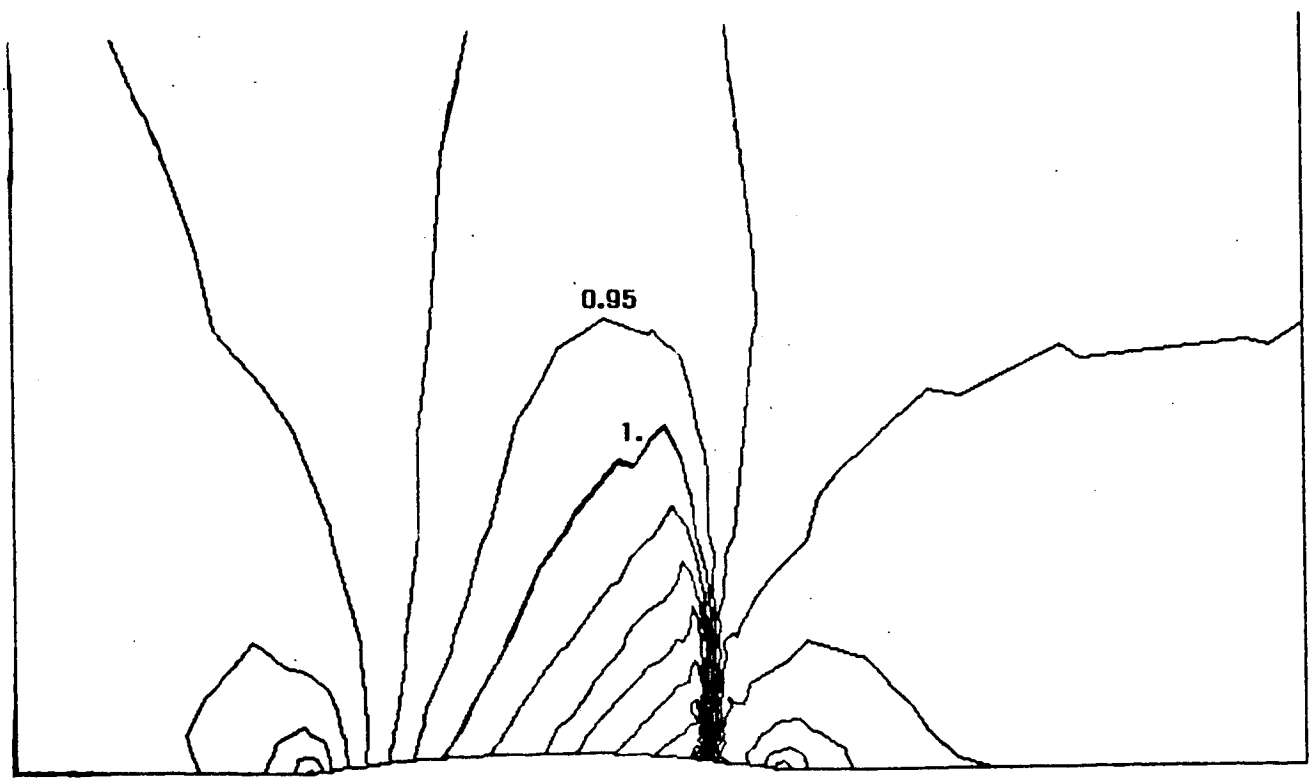

Figure 6.28 Corresponding Blow-up of the Mach contours

MIN : -.4390544E+00 - MAX : 0.8193751E+00

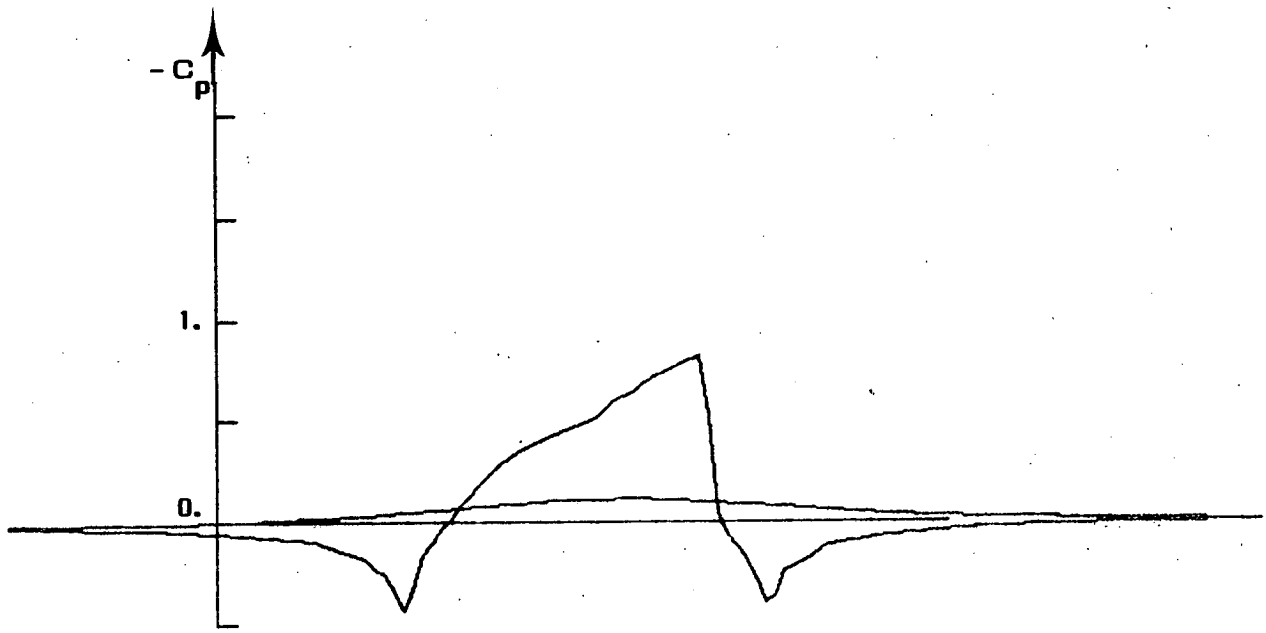

Figure 6.29 Pressure

MIN : -.1271314E-01 - MAX : 0.1549686E-01

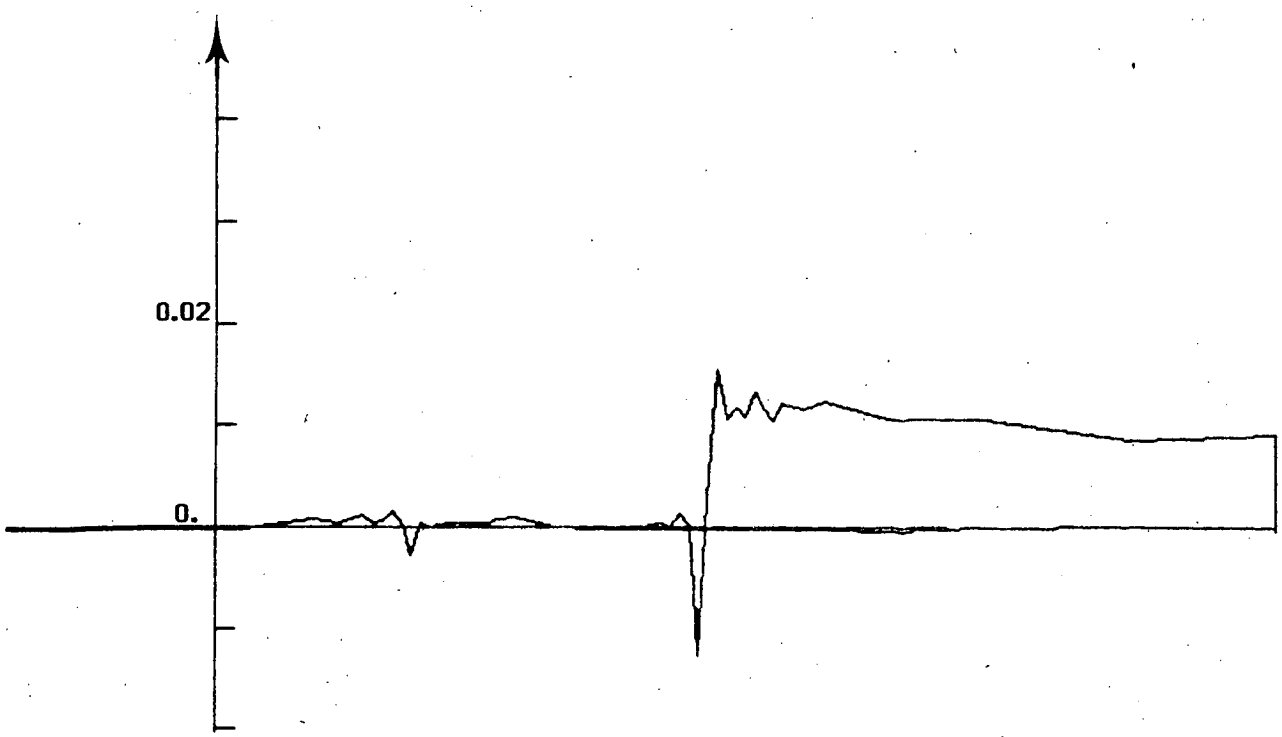

Figure 6.30 Entropy

7 NACA 0012 AIRFOIL

7.1 Model problem-coarse mesh

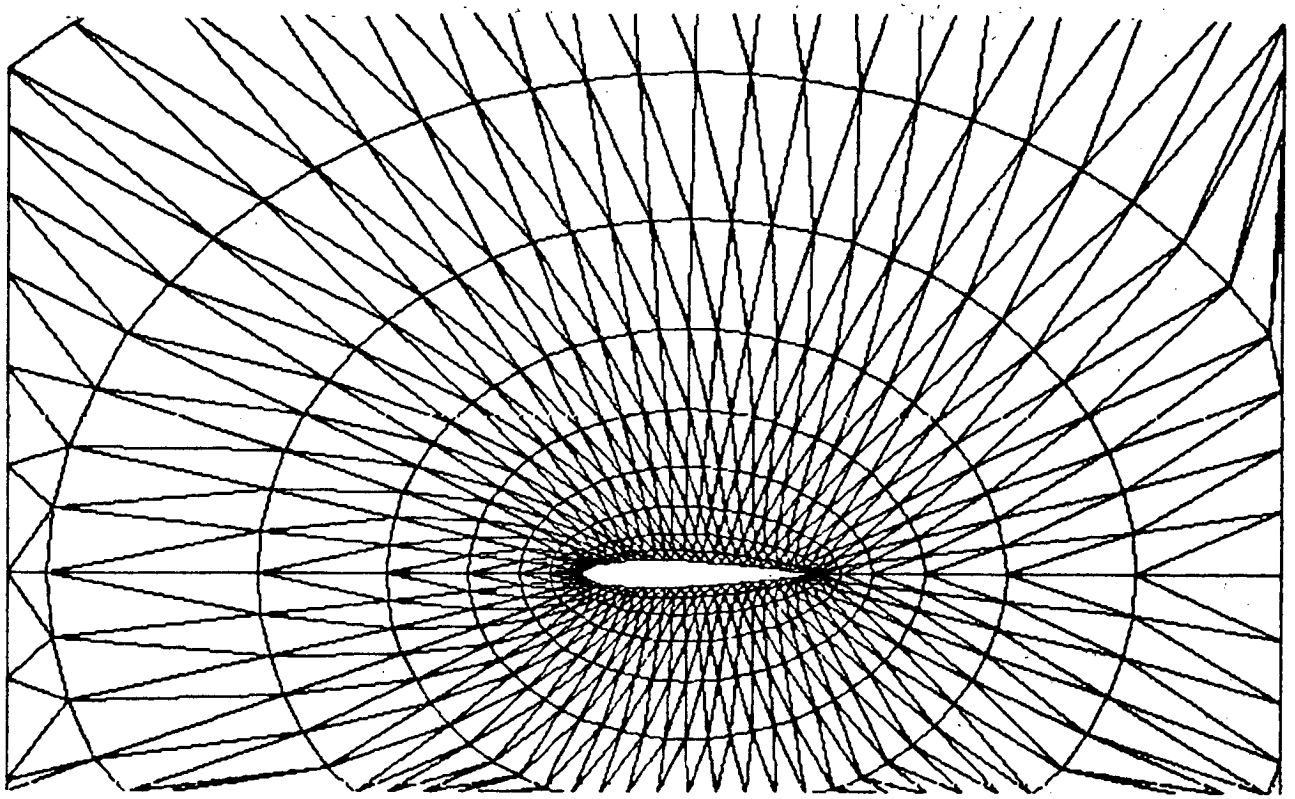

Figure 7.1 Coarse mesh (600 points)

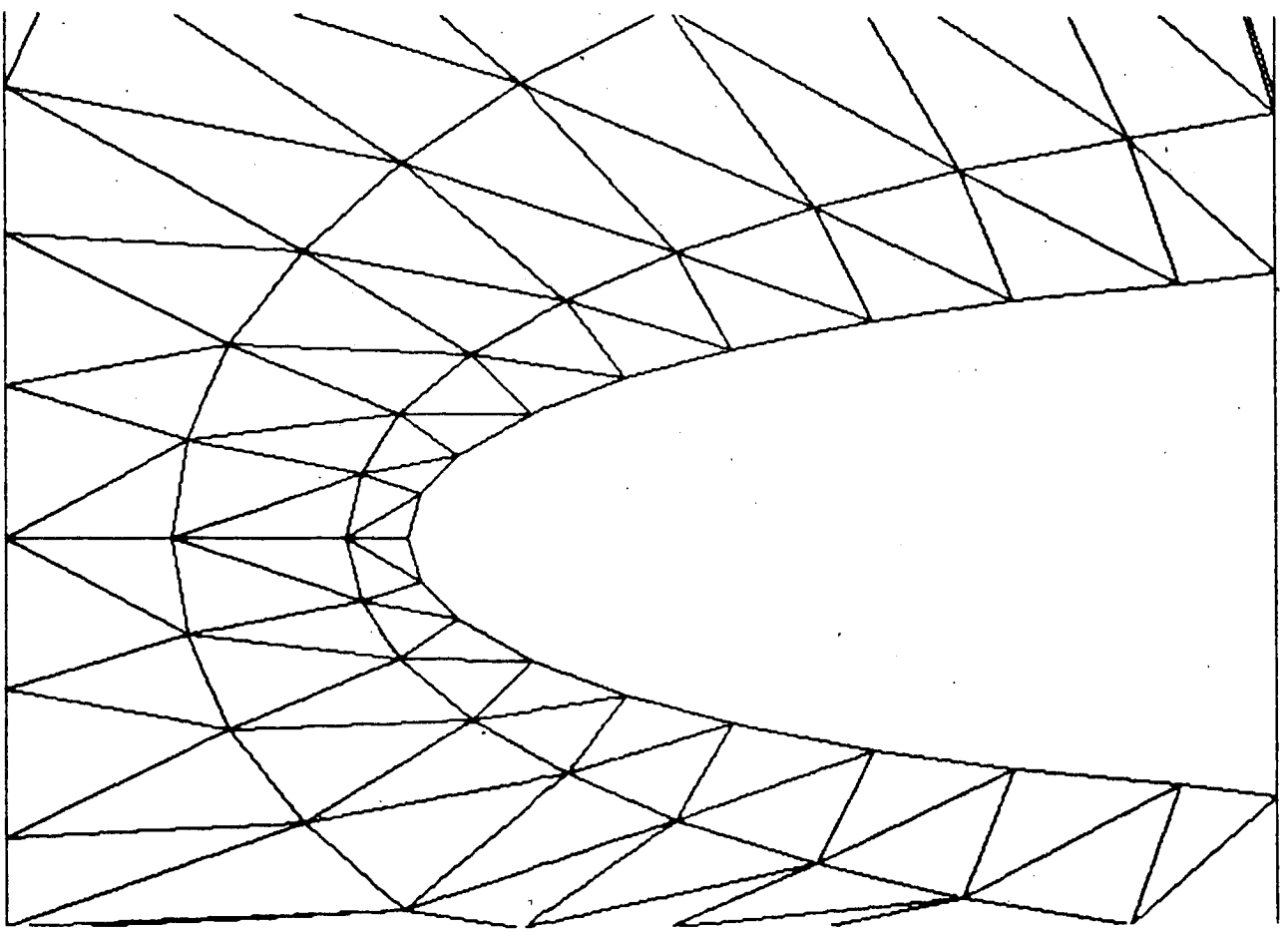

Figure 7.2 Blow-up of the mesh in front of the airfoil

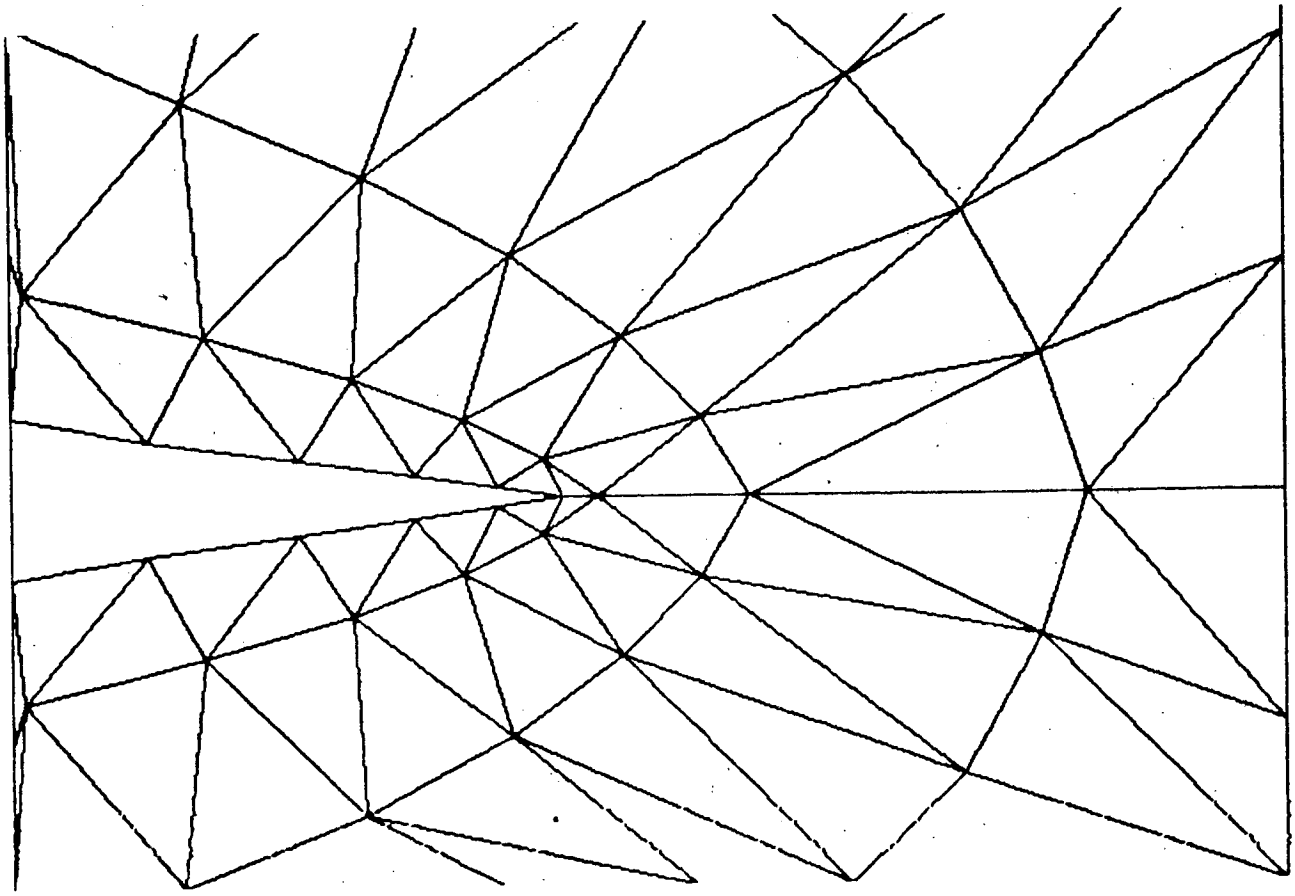

Figure 7.3 Blow-up of the mesh at the near of the airfoil

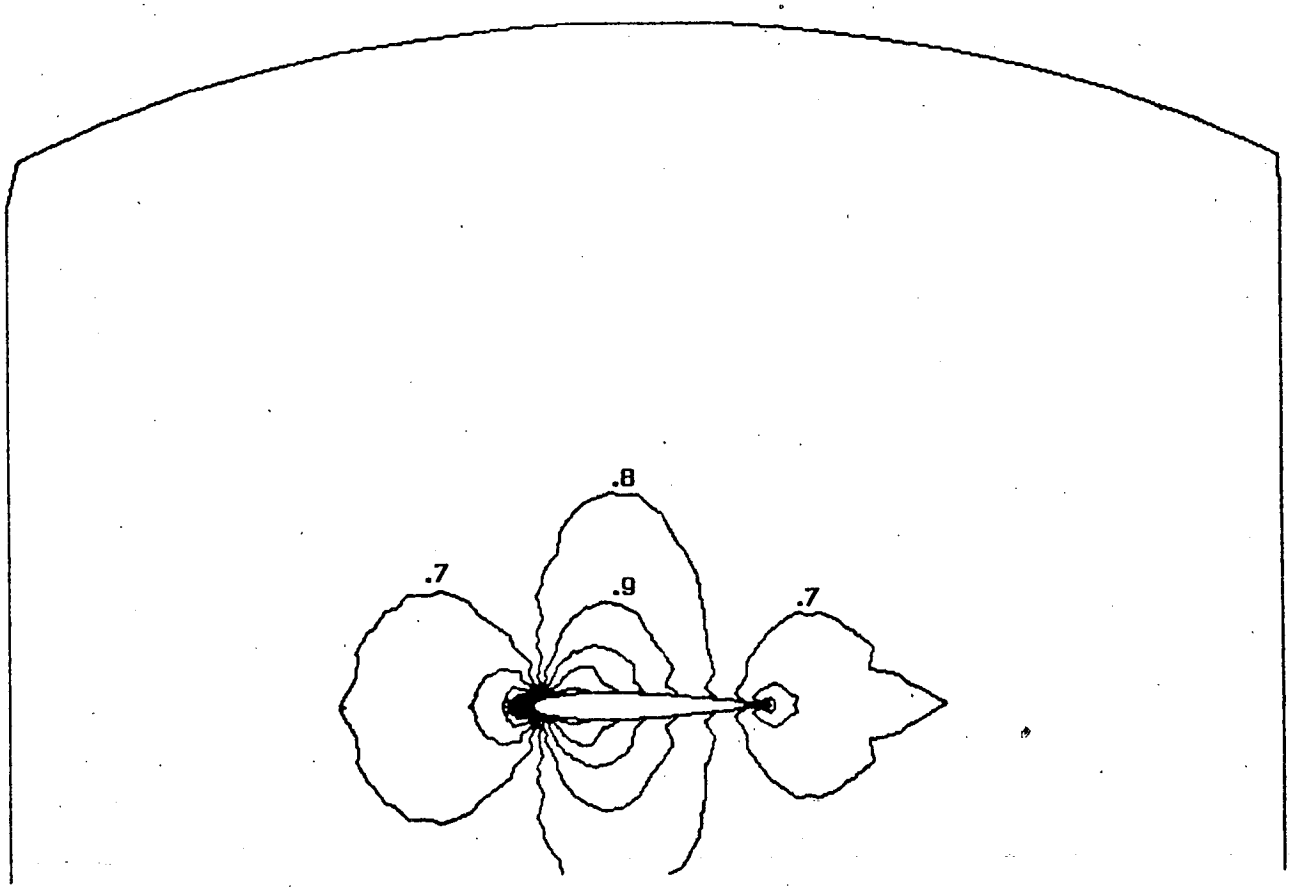

Figure 7.4 Mach contours

MIN : -.9302911E+00 - MAX : 0.6388564E+00

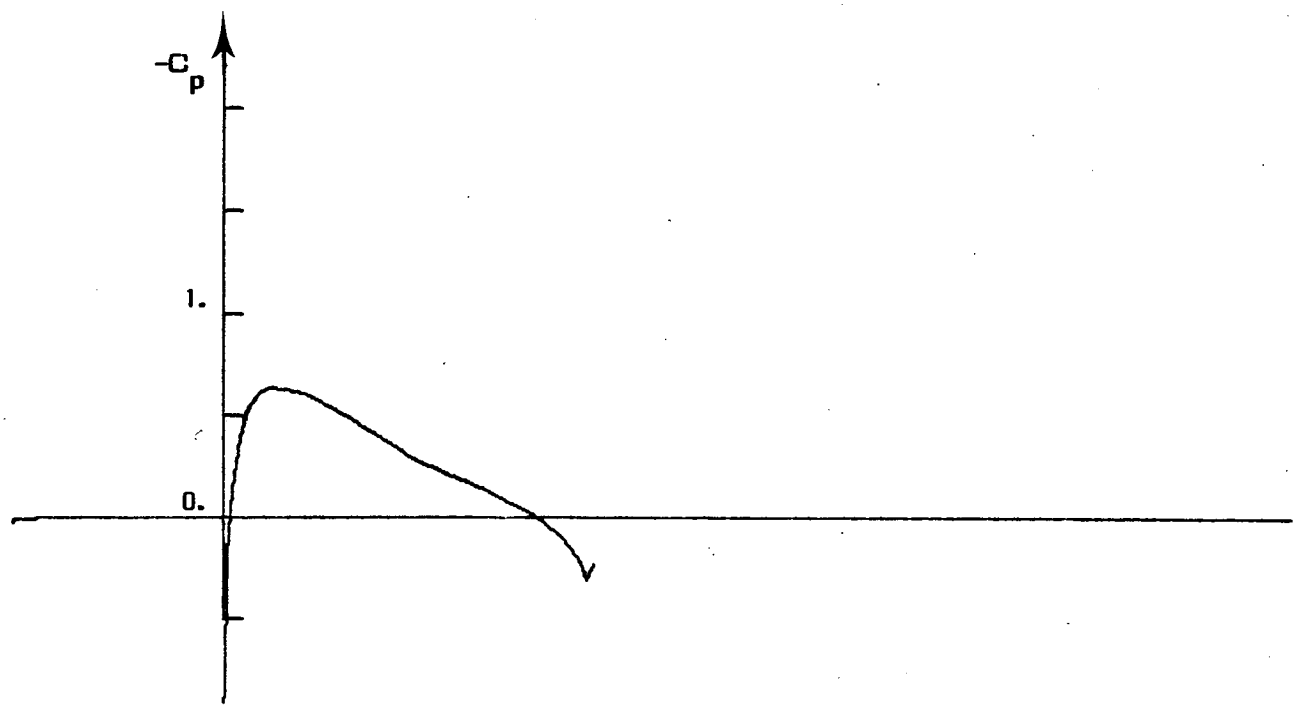

Figure 7.5 Pressure

MIN : -.1071563E-01 - MAX : 0.2186339E-01

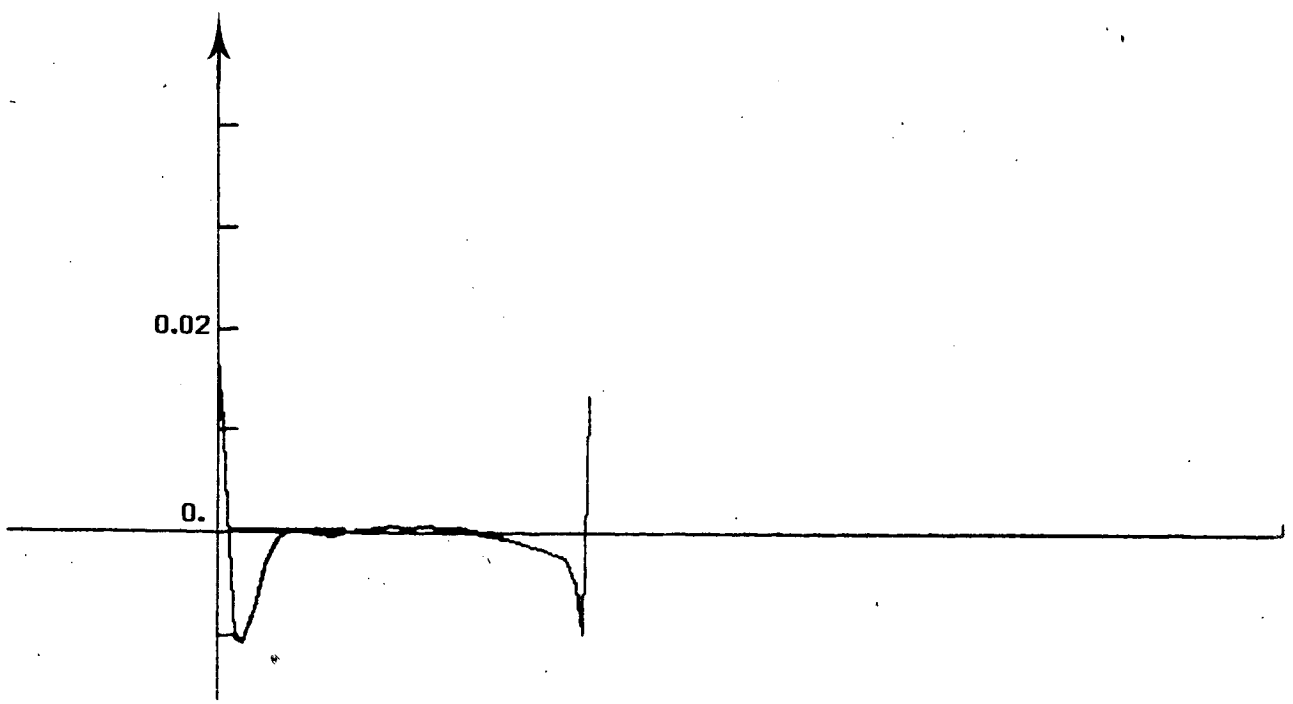

Figure 7.6 Entropy

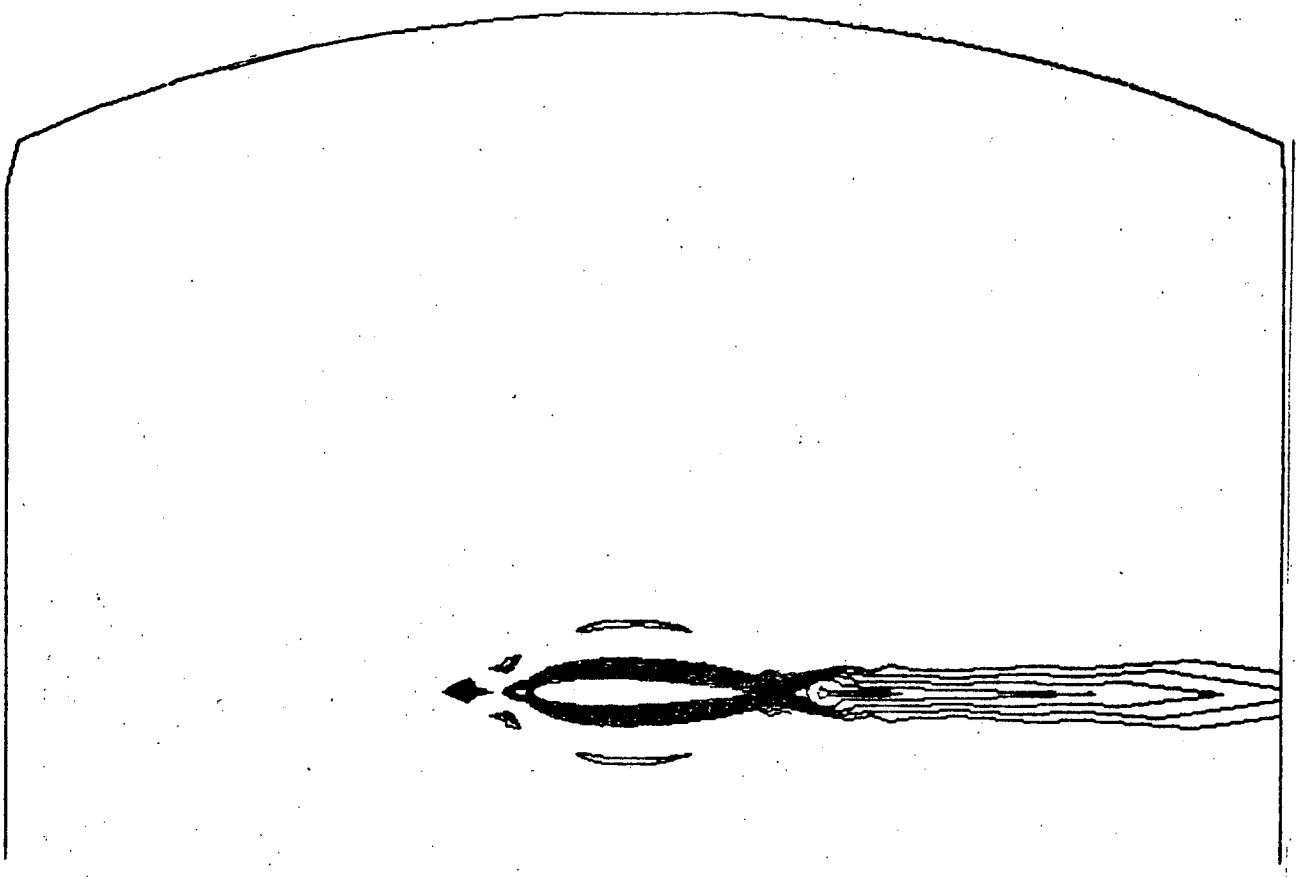

Figure 7.7 Entropy contours ($\Delta s = 0.001$)

7.2 Results obtained using geometrical test

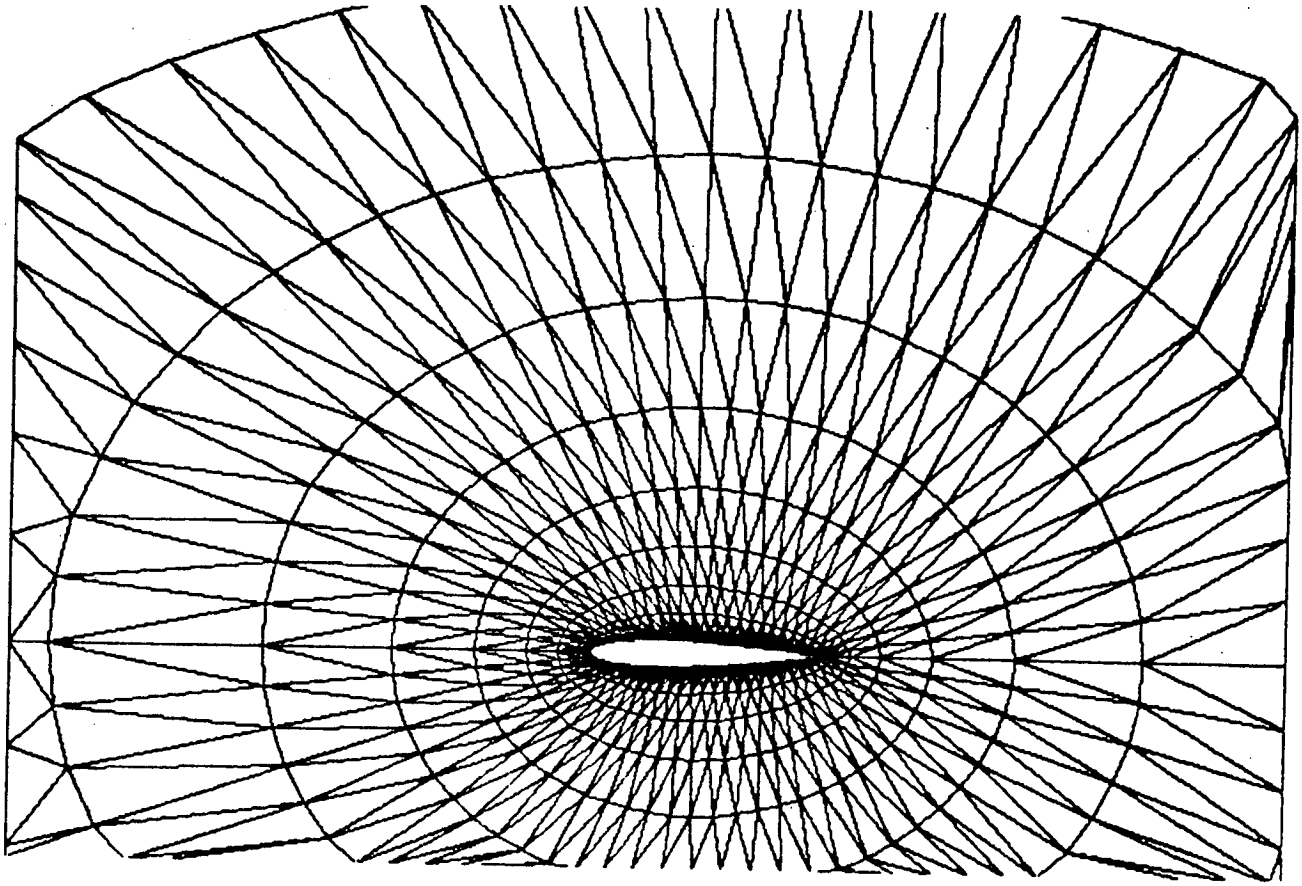

Figure 7.8 Final mesh (840 points)

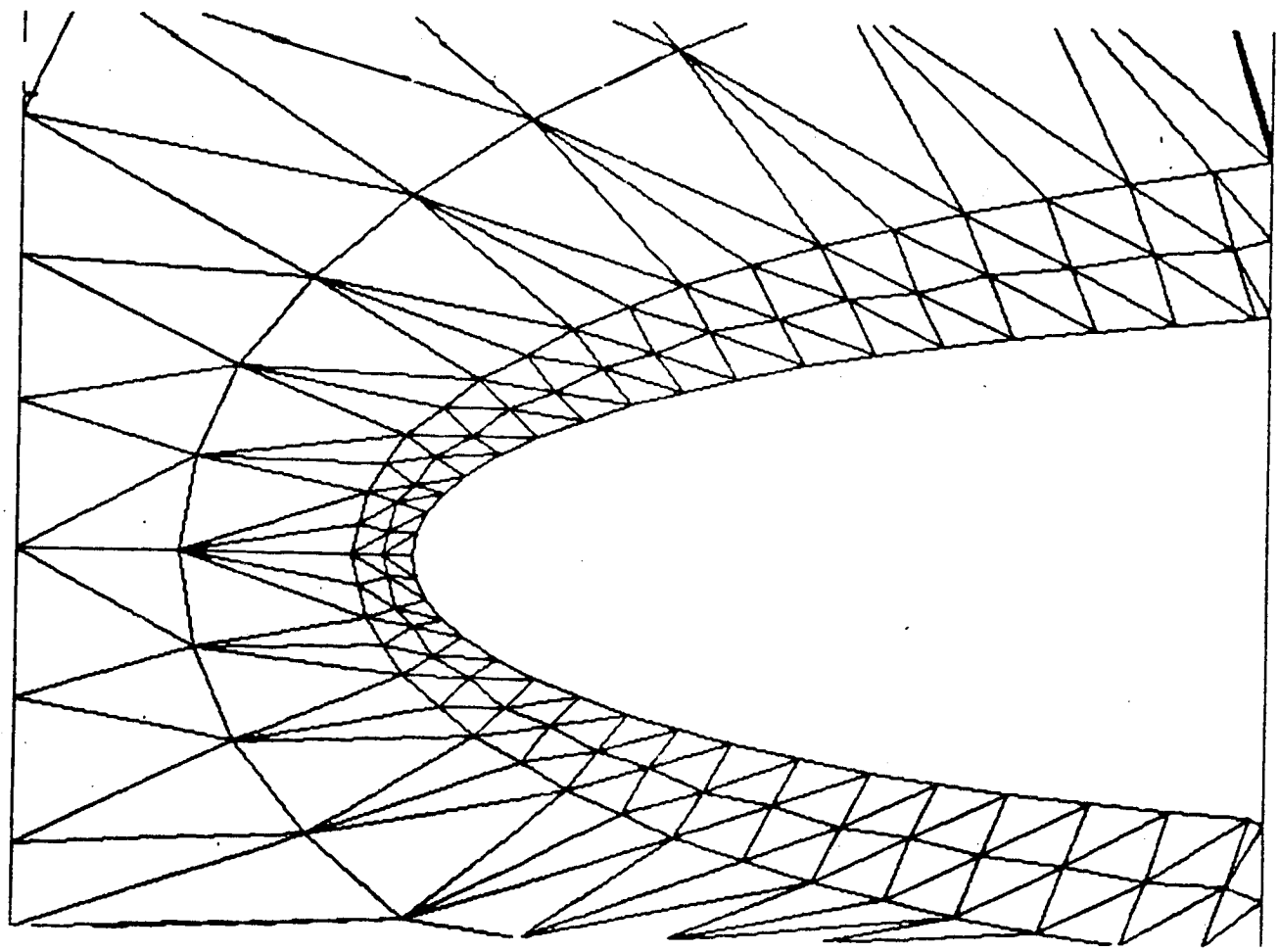

Figure 7.9 Blow-up of the mesh in front of the airfoil

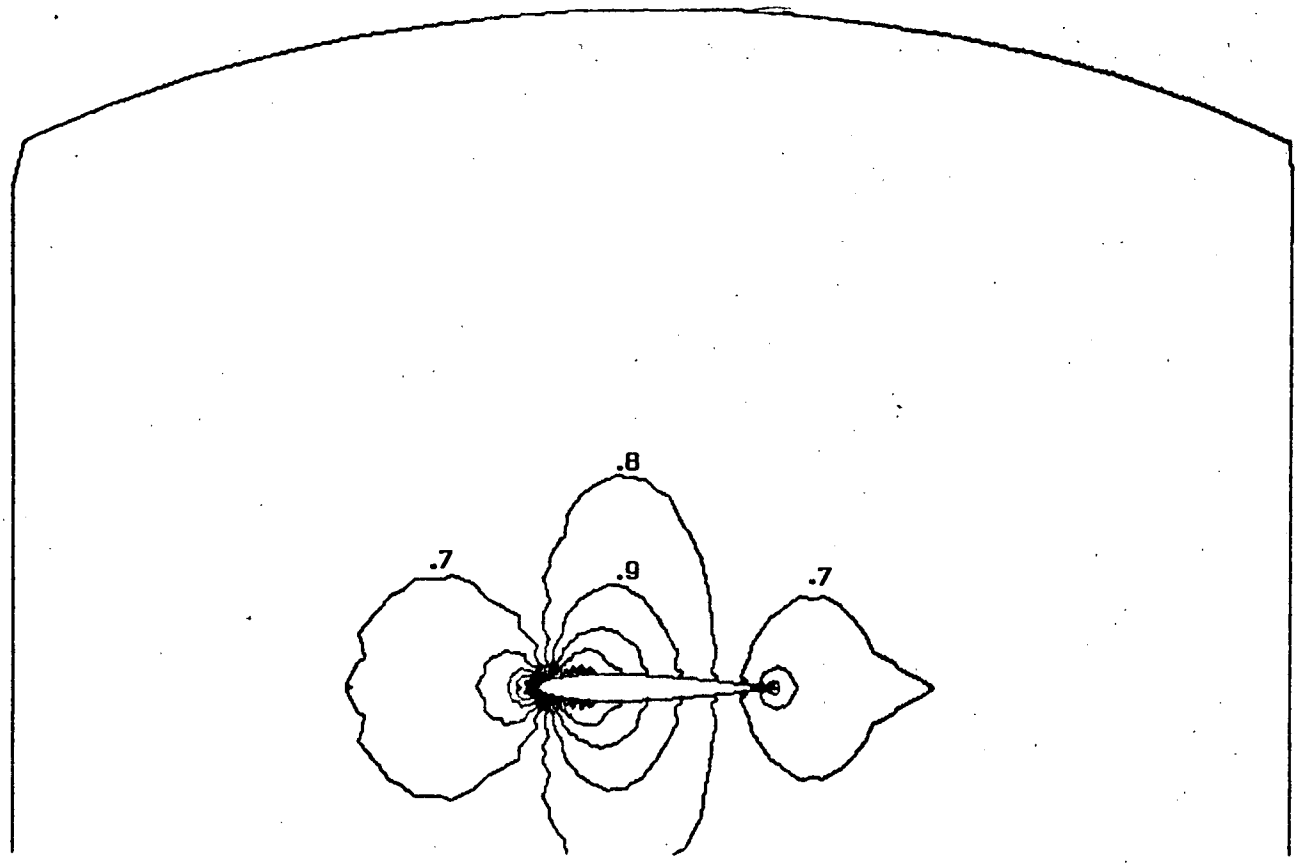

Figure 7.10 Mach contours

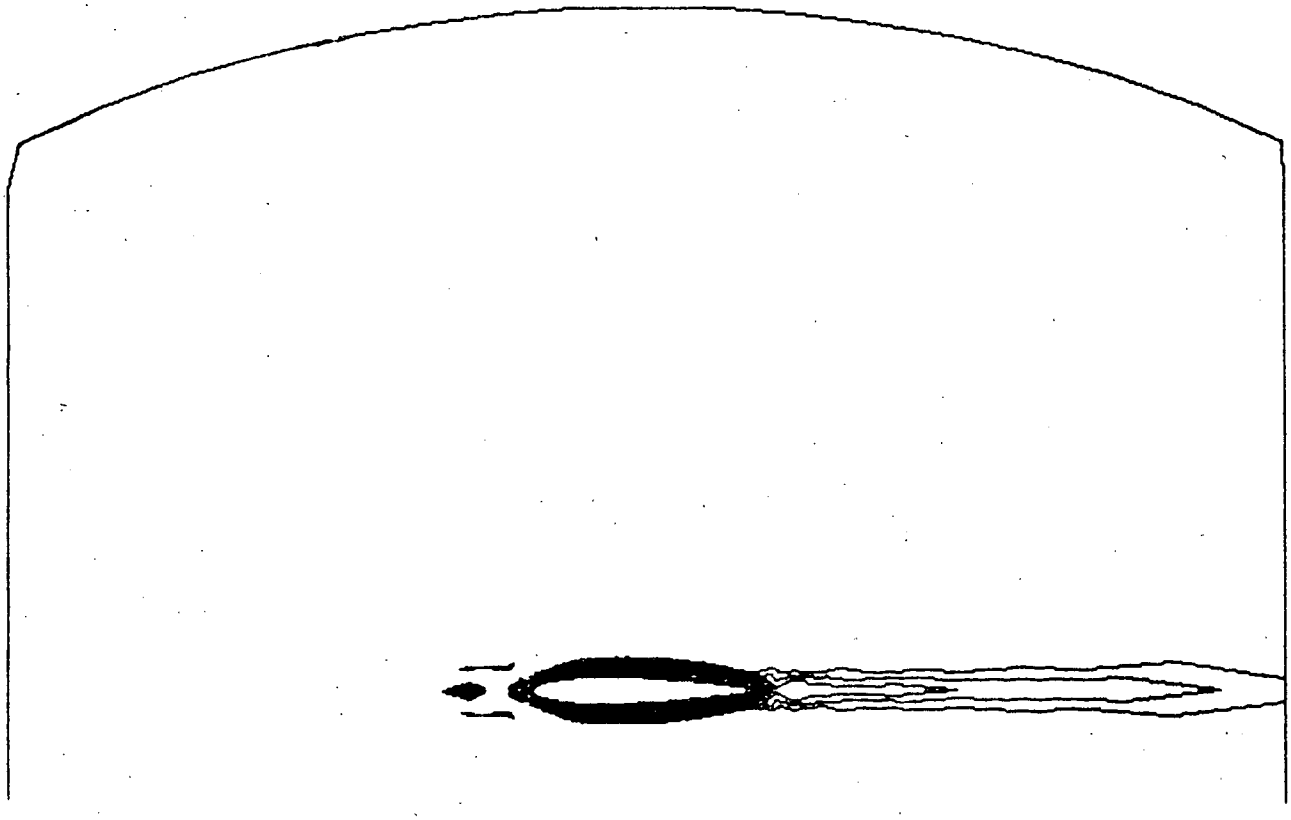

Figure 7.11 Entropy contours ($\Delta s = 0.001$)

MIN : -.9561259E+00 - MAX : 0.6745808E+00

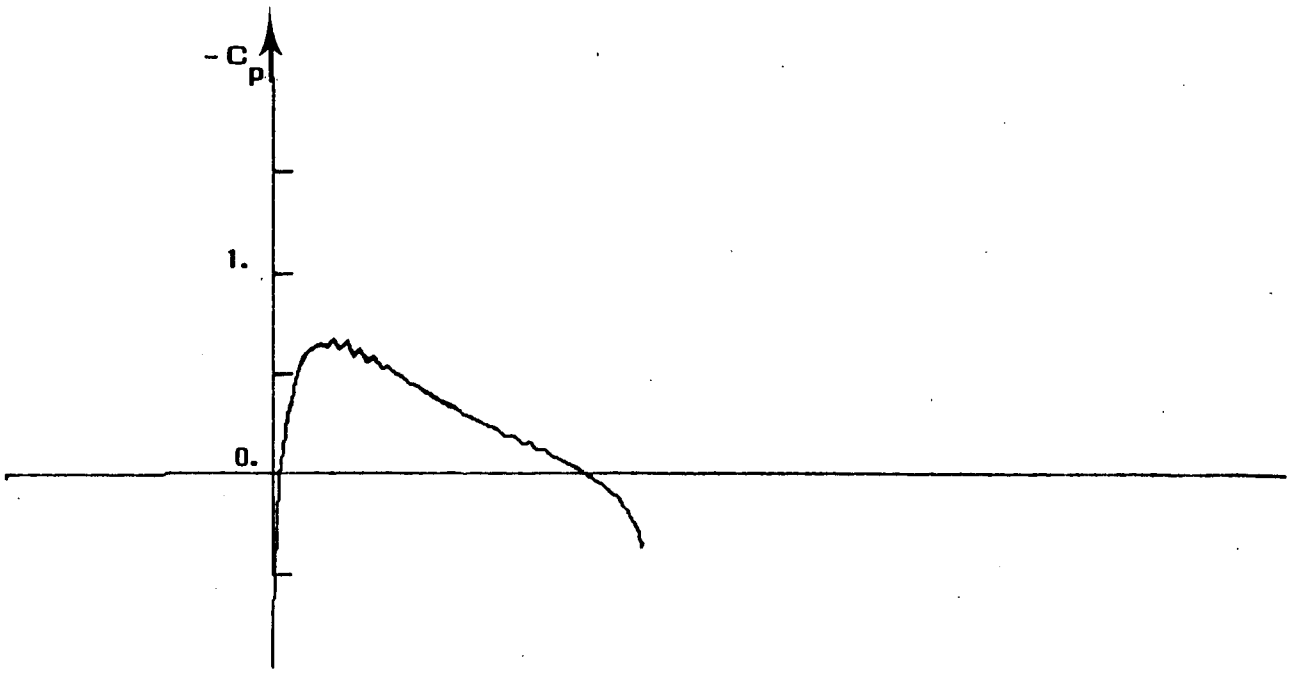

Figure 7.12 Pressure

MIN : -.3262222E-04 - MAX : 0.2999037E-01

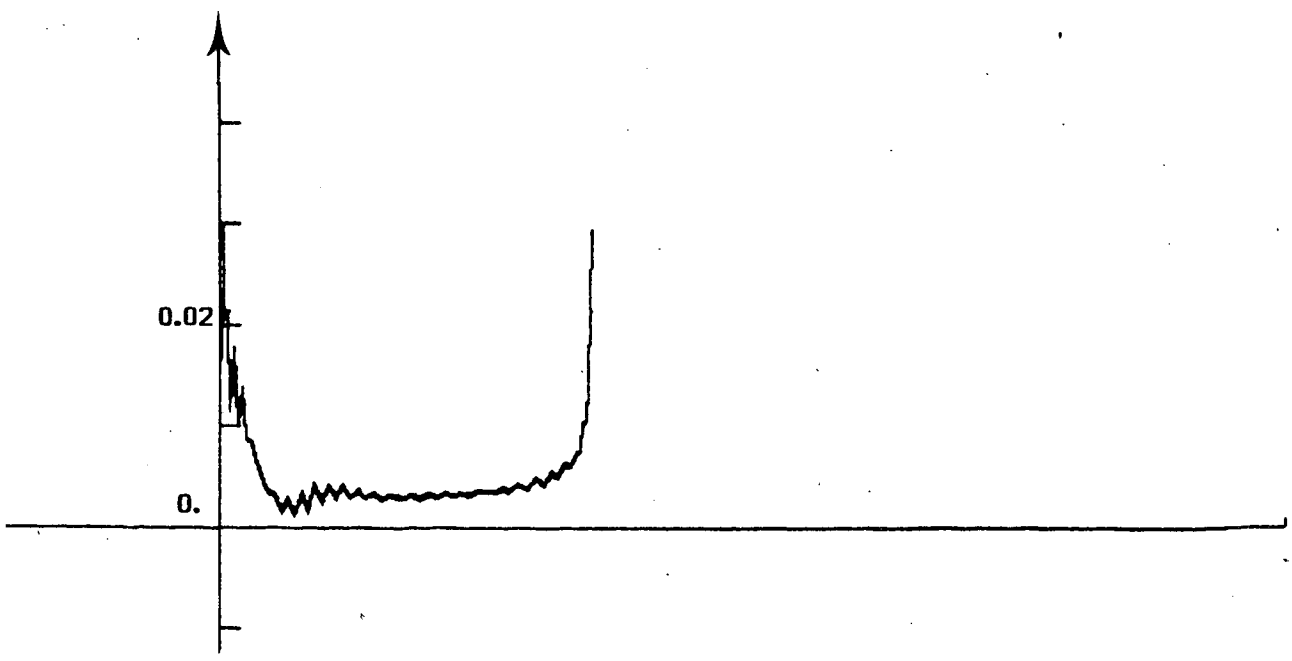

Figure 7.13 Entropy

7.3 Results obtained using the test on the error estimate

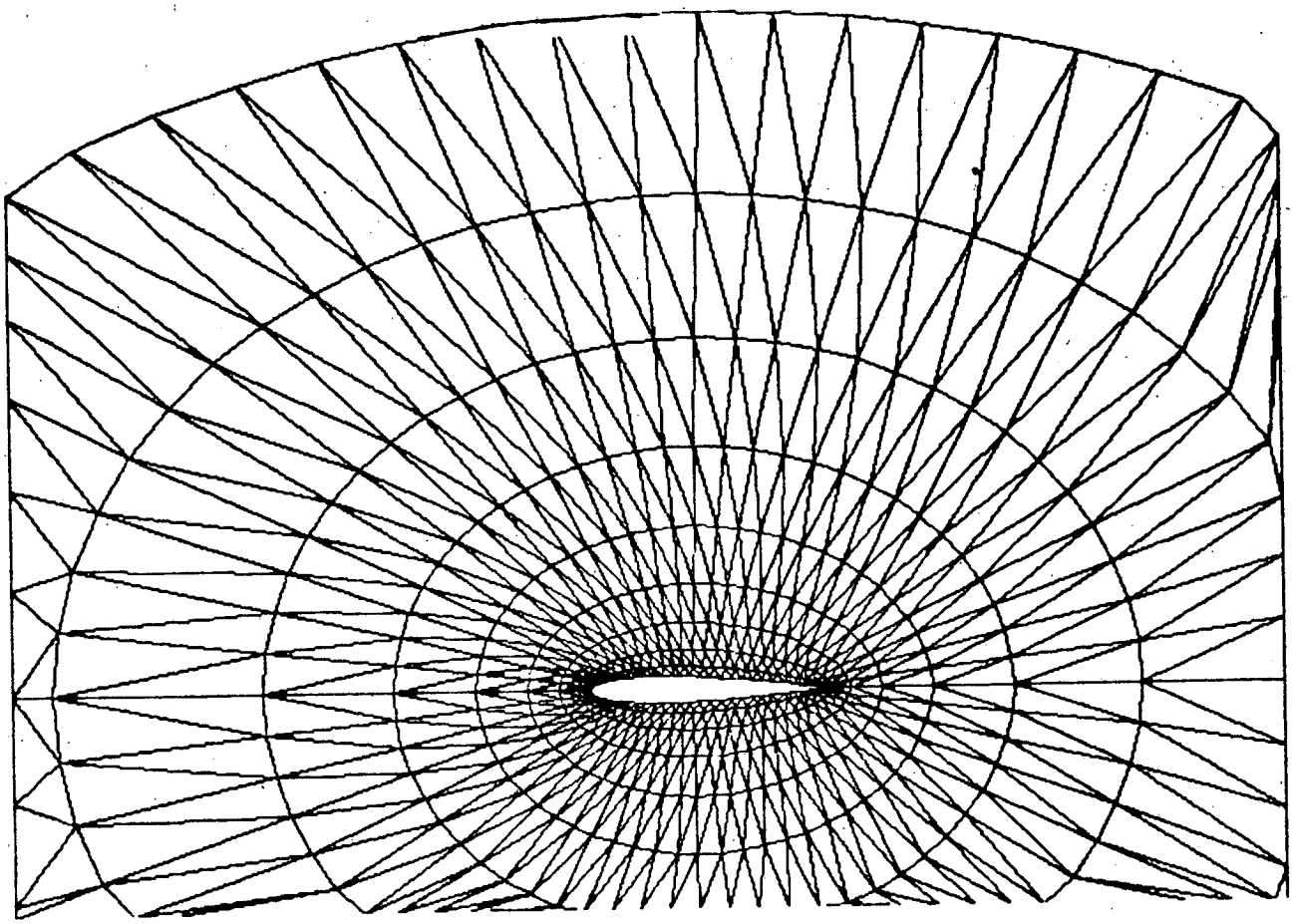

Figure 7.14 Final mesh (678 points)

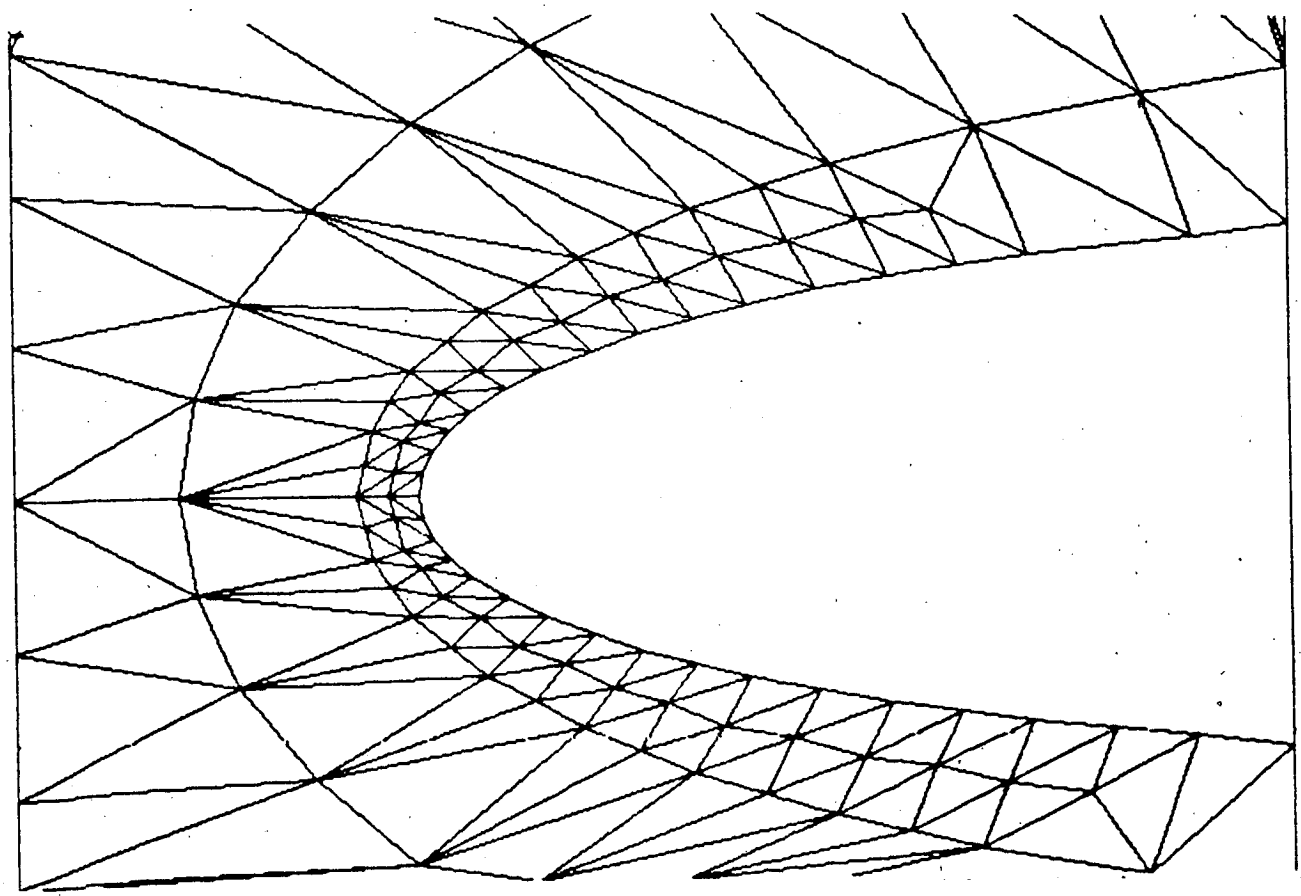

Figure 7.15 Blow-up of the mesh in front of the airfoil

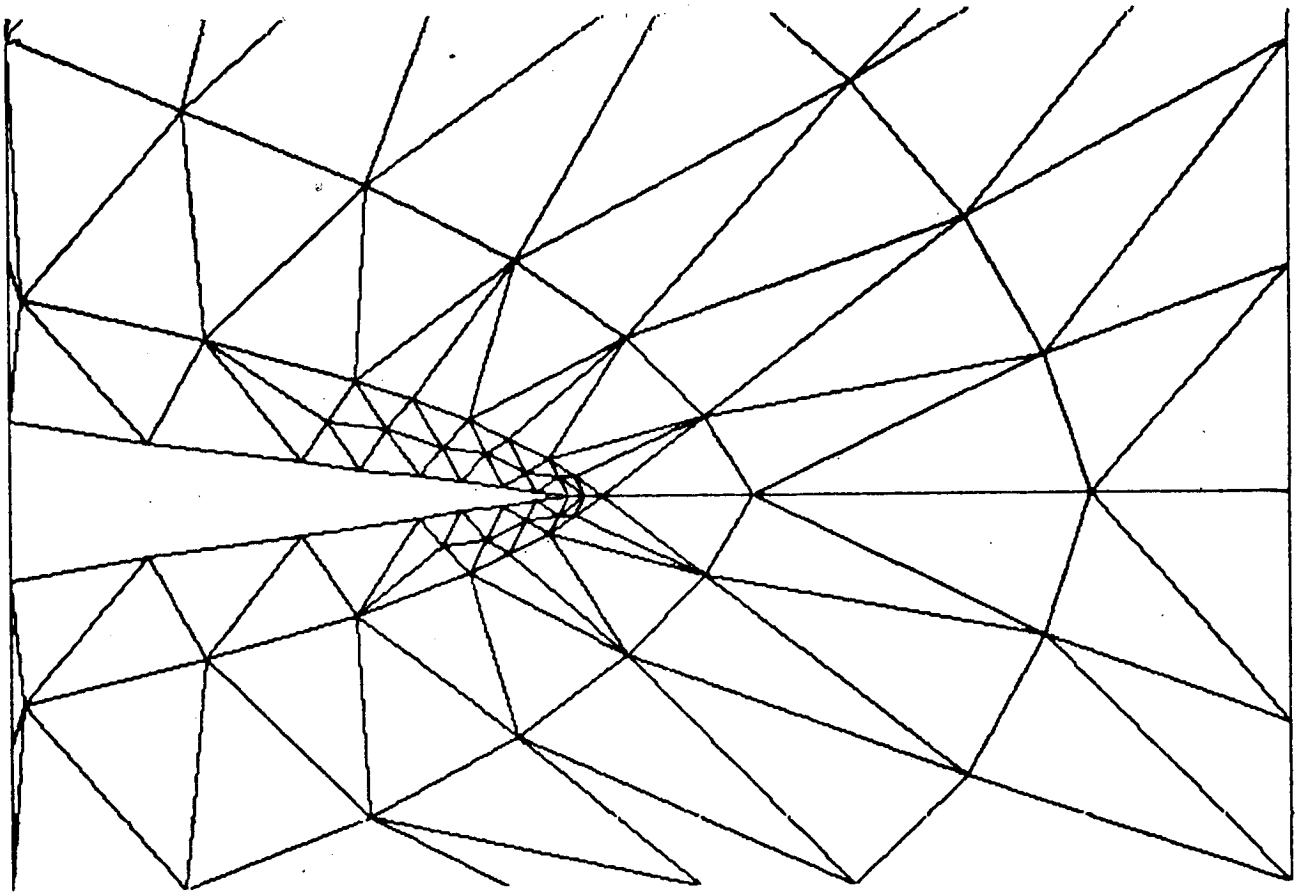

Figure 7.16 Blow-up of the mesh at the near of the airfoil

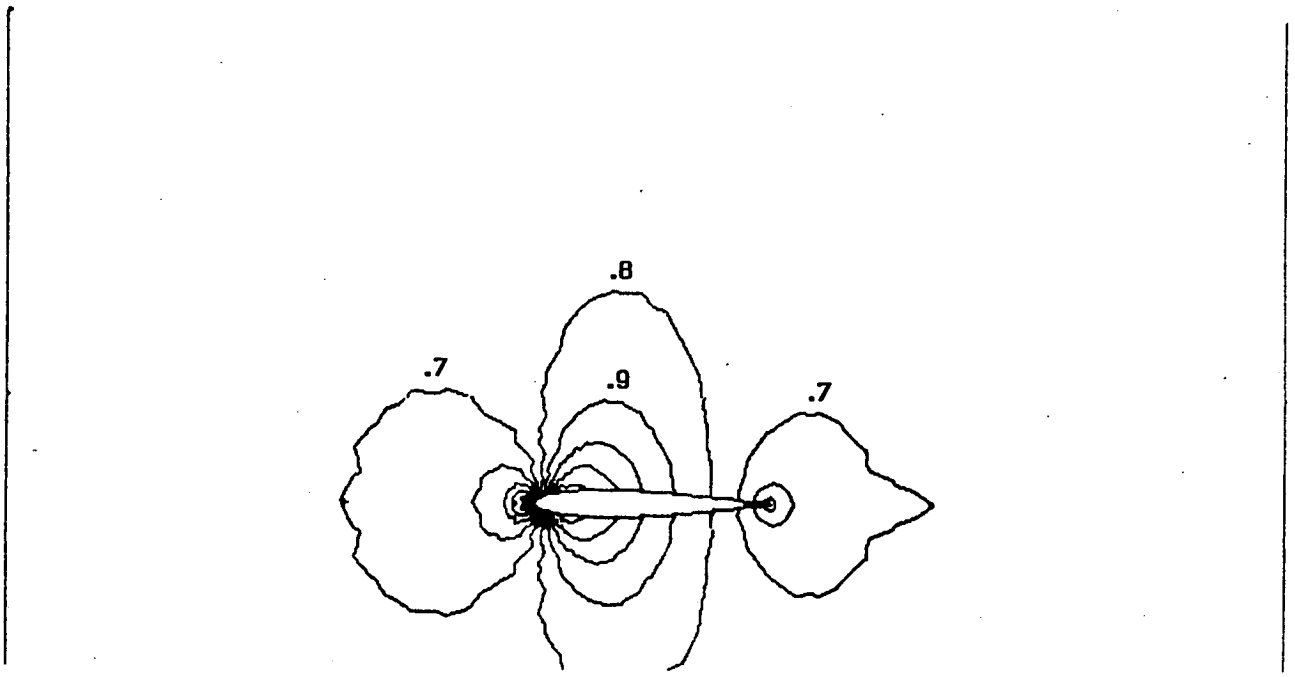

Figure 7.17 Mach contours

MIN : -.9516305E+00 - MAX : 0.6699146E+00

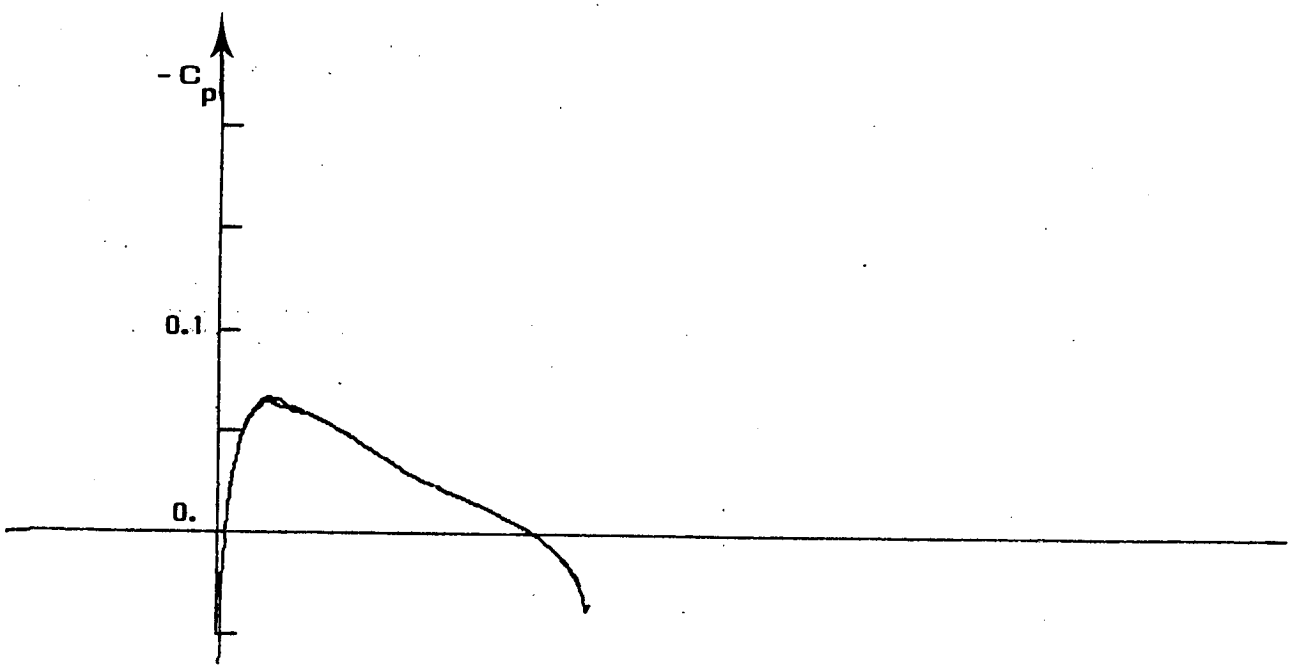

Figure 7.18 Pressure

MIN : -.3262161E-04 - MAX : 0.3042167E-01

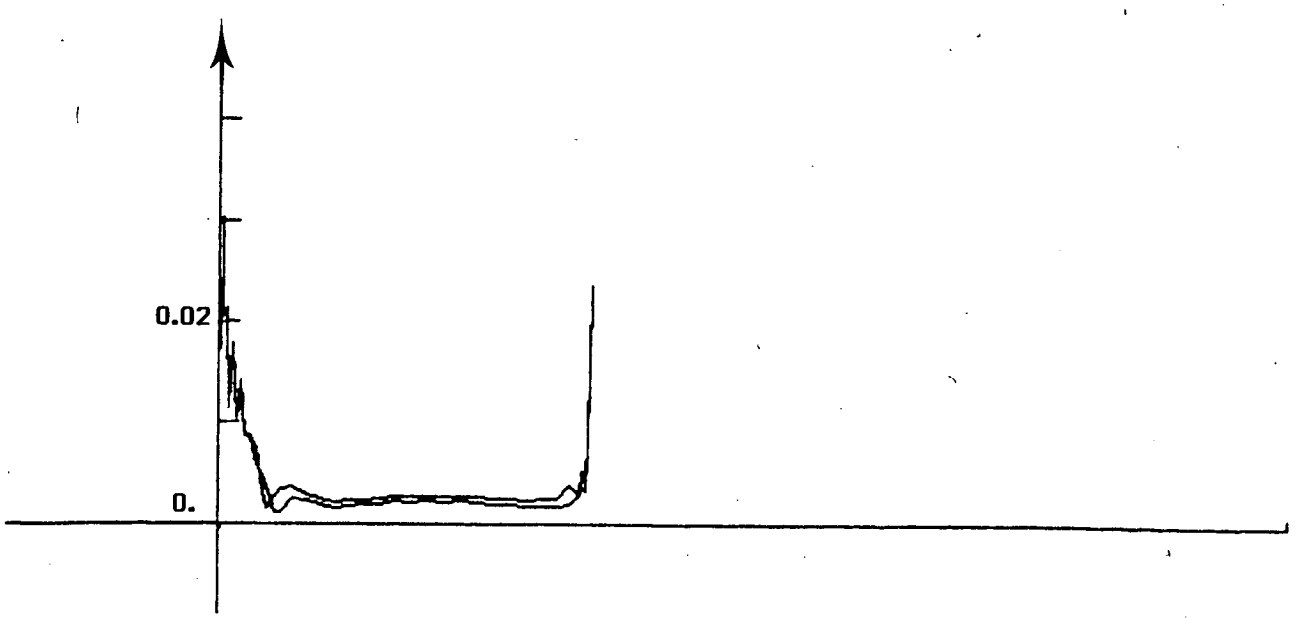

Figure 7.19 Entropy

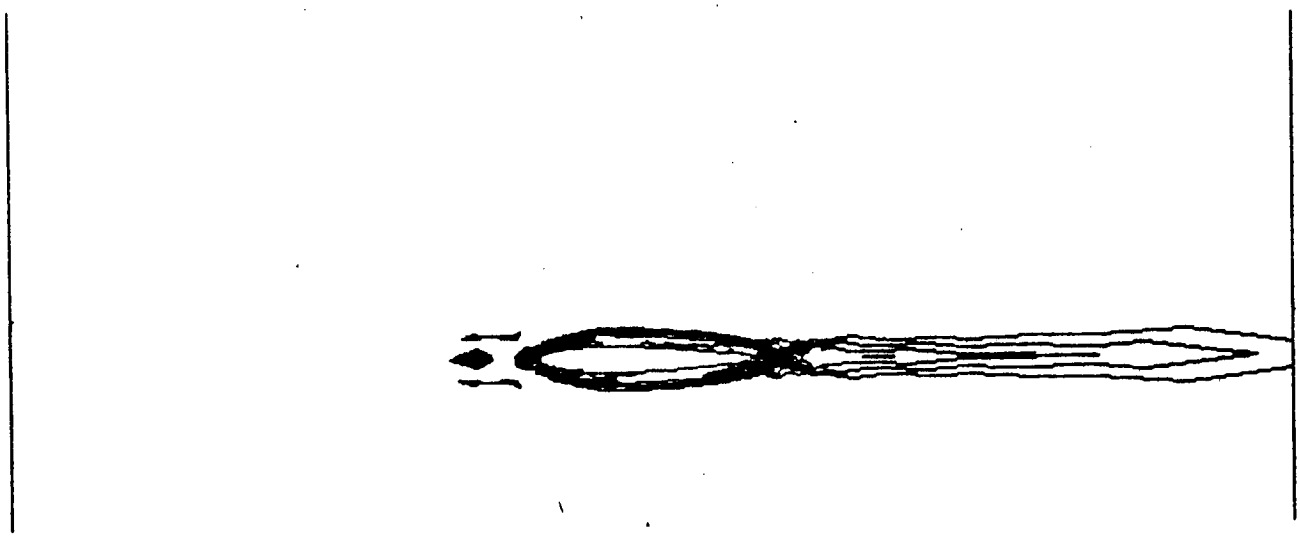

Figure 7.29 Entropy contours ($\Delta s = 0.001$)

7.4 Results obtained using the test on the entropy

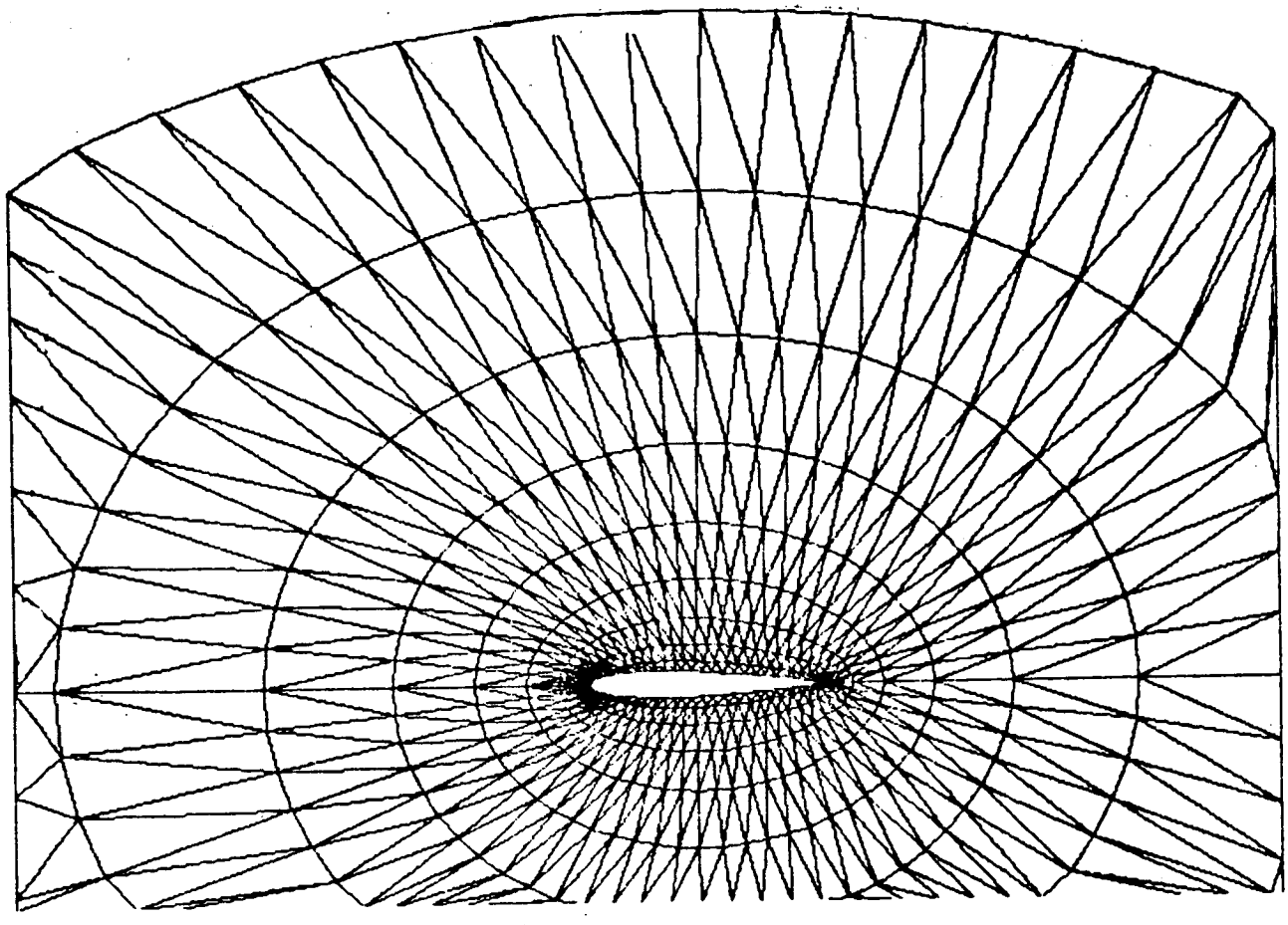

Figure 7.21 Final mesh (735 points)

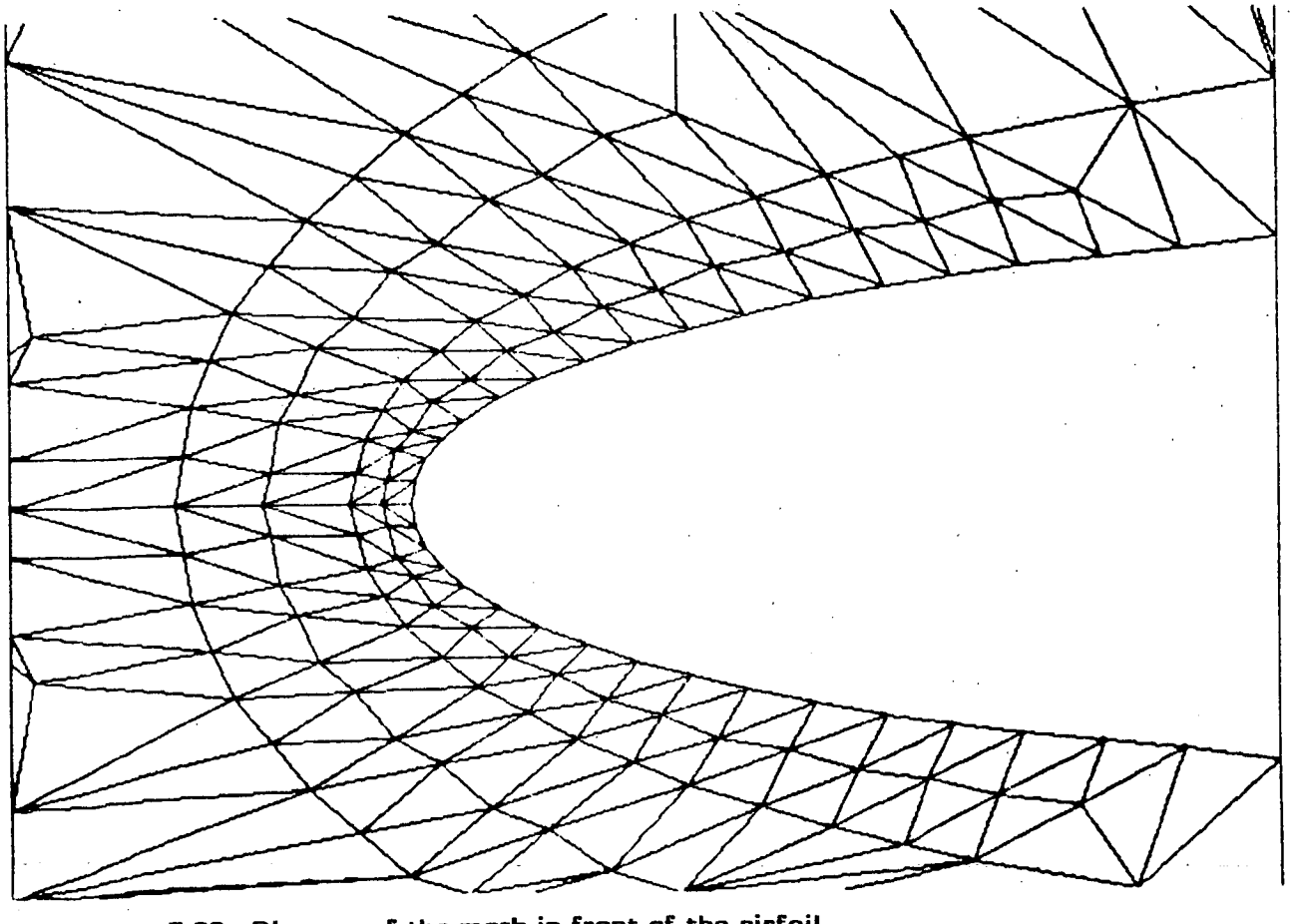

Figure 7.22 Blow-up of the mesh in front of the airfoil

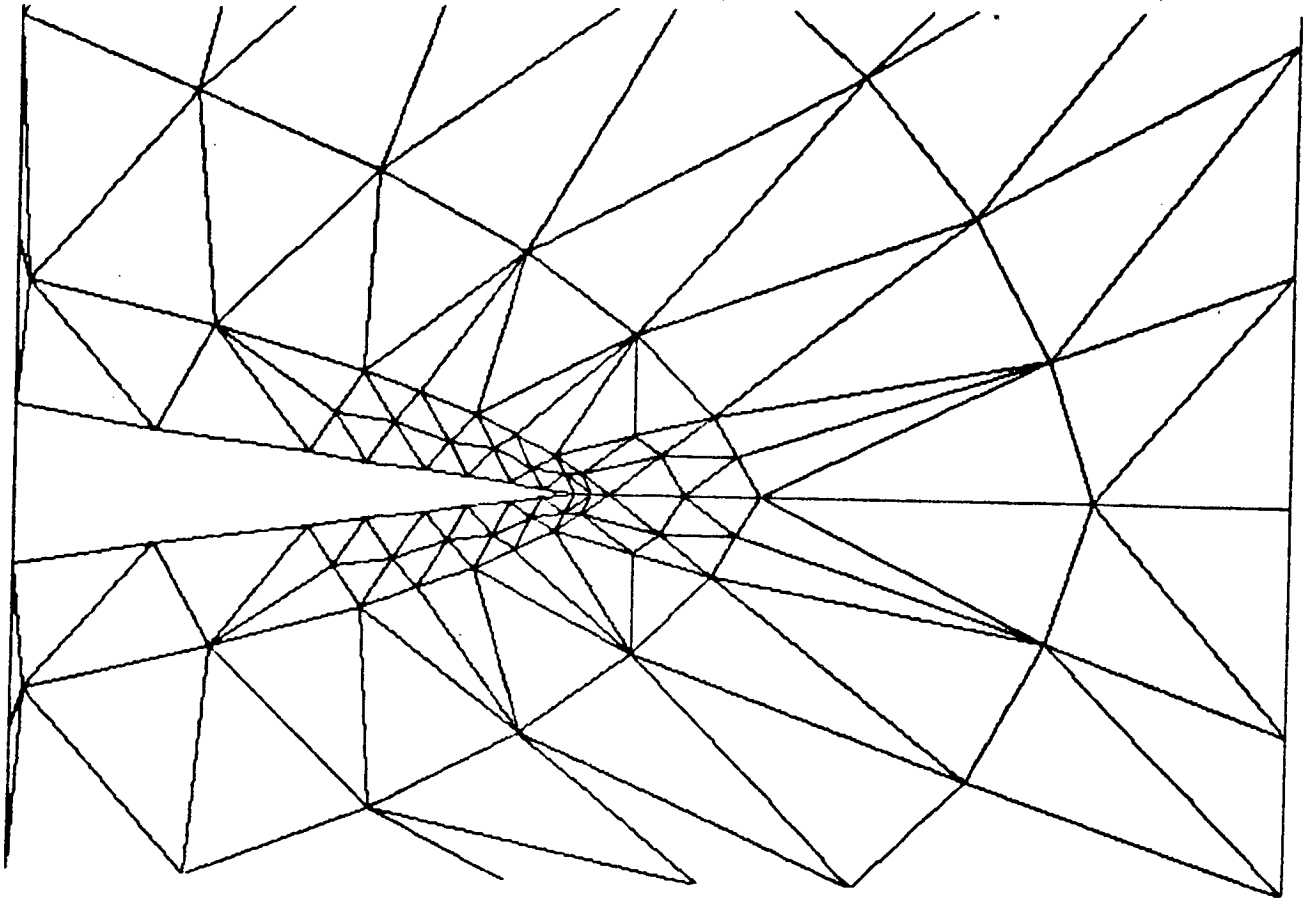

Figure 7.23 Blow-up of the mesh at the near of the airfoil

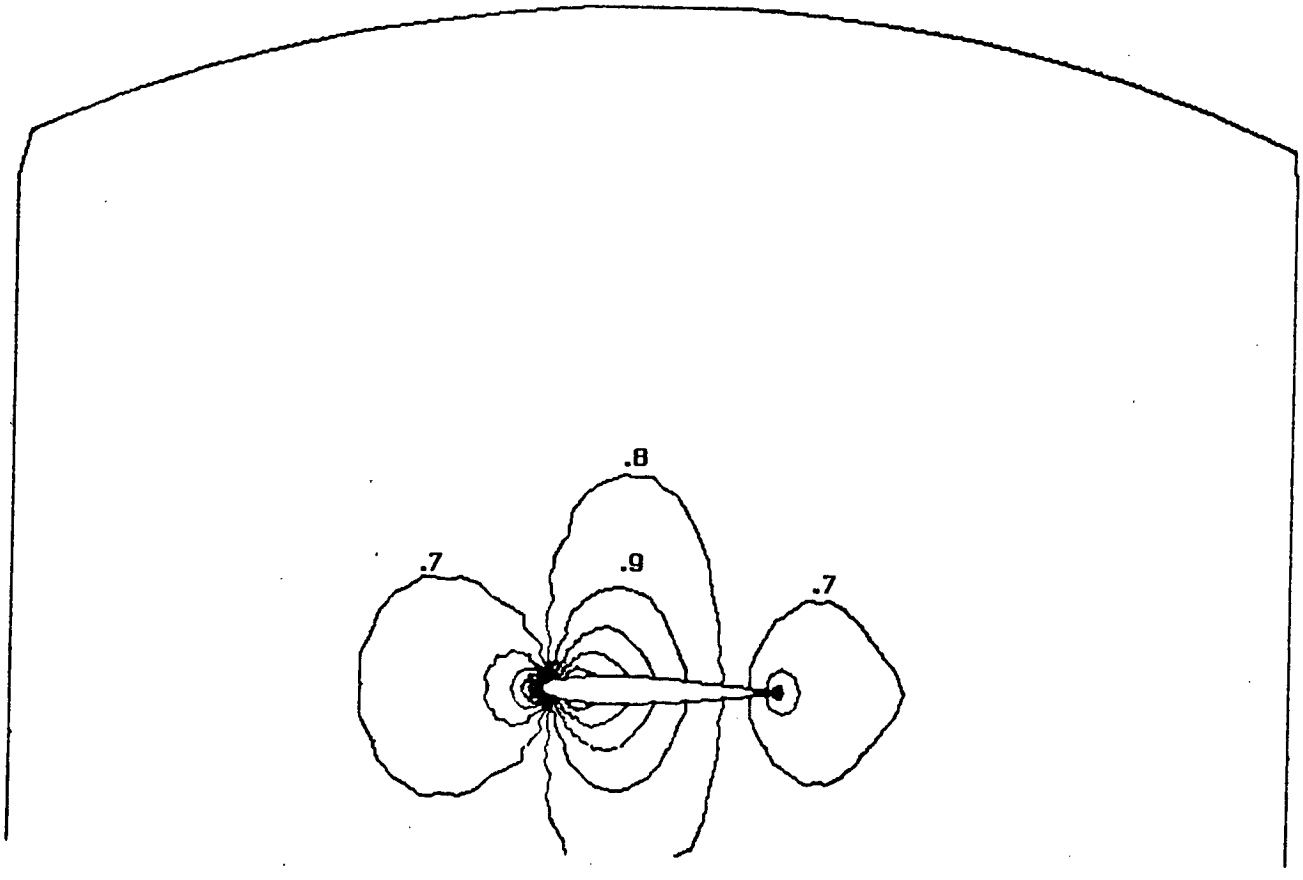

Figure 7.24 Mach contours

MIN : -.1129672E+01 - MAX : 0.6631688E+00

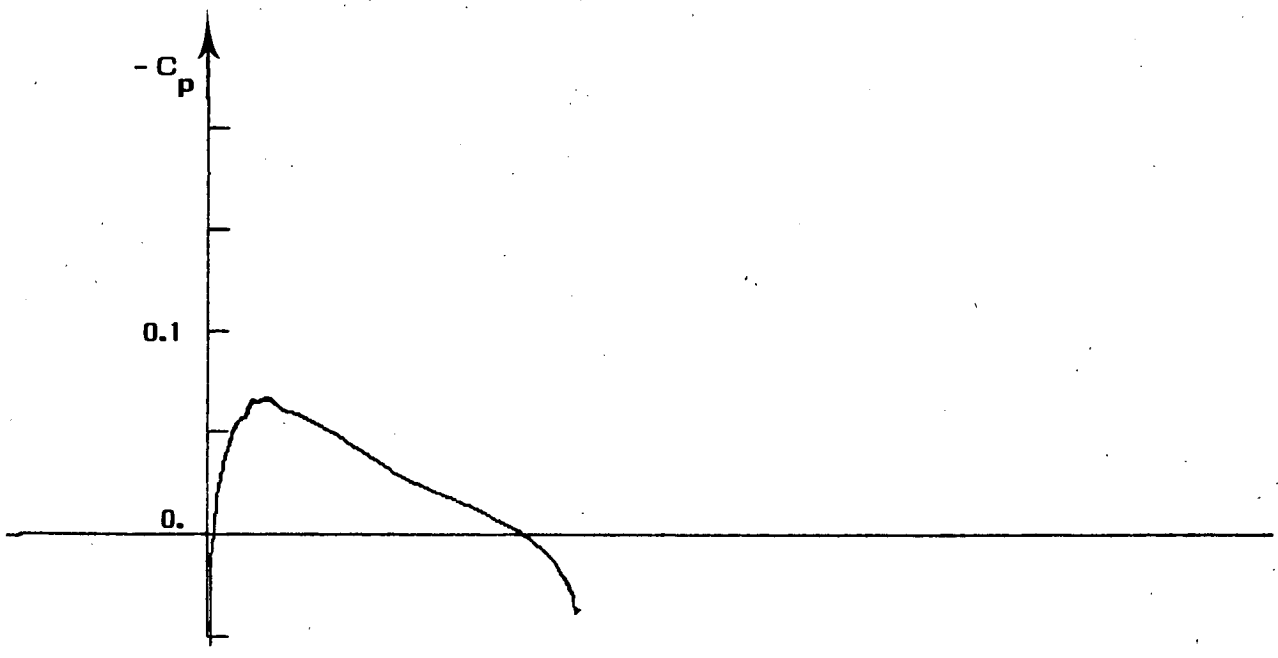

Figure 7.25 Pressure

MIN : -.3496722E-02 - MAX : 0.2135553E-01

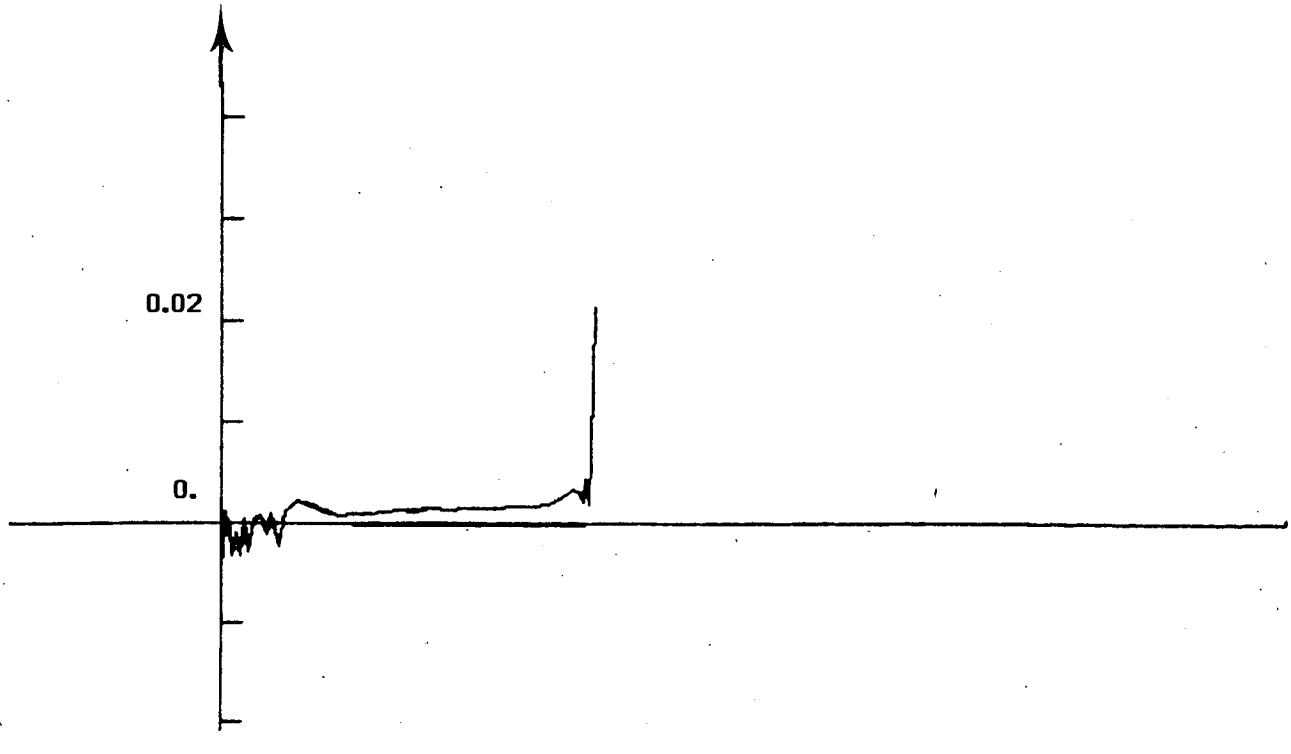

Figure 7.26 Entropy

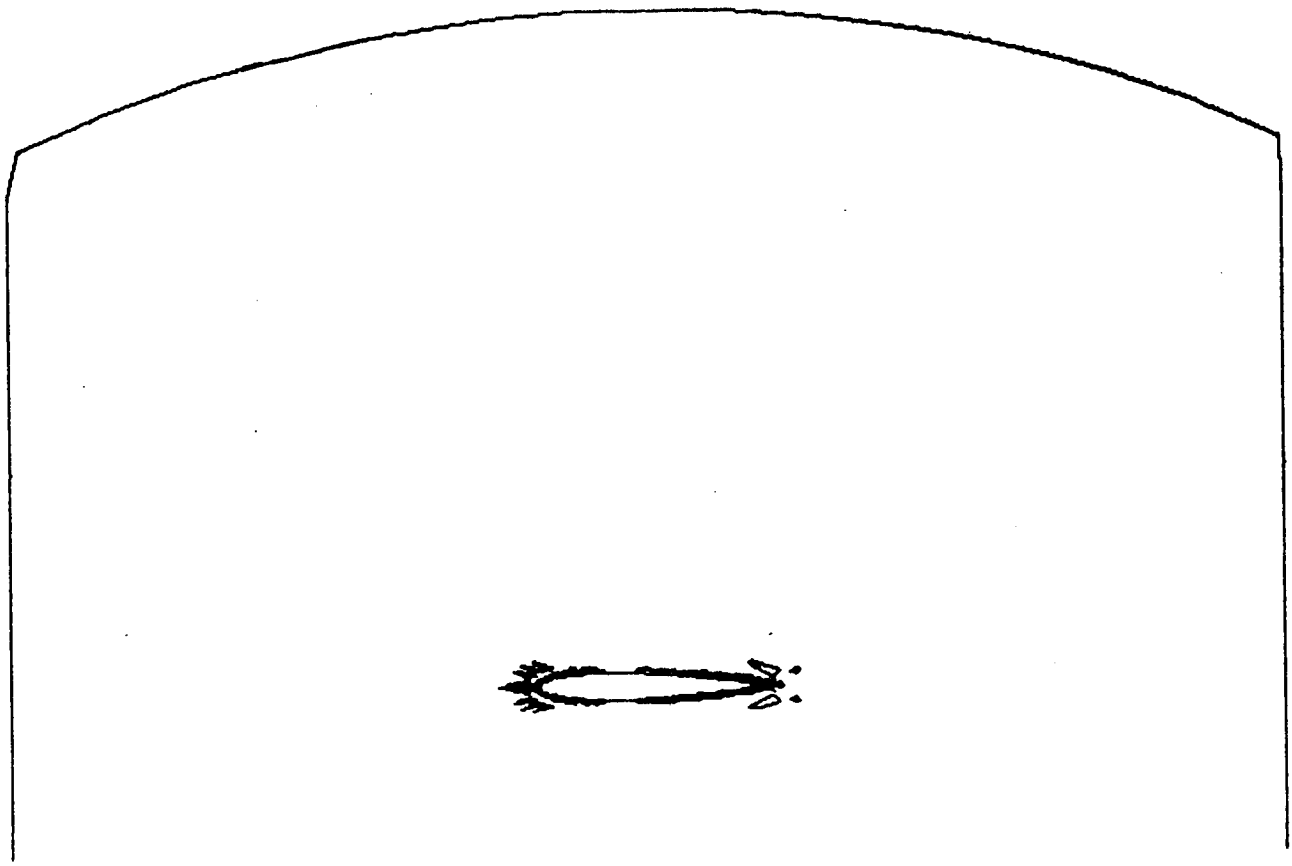

Figure 7.27 Entropy contours ($\Delta s = 0.001$)

REFERENCES

{1} D.A. ANDERSON, "Adaptive Mesh Schemes Based on Grid Speeds", AIAA Comp. Fluid Dynamic Conference, Danvers, Massachusetts, July 13-15, 1983.

{2} F. ANGRAND, A. DERVIEUX, "Some Explicit Triangular Finite Element Schemes for the Euler Equations", International Journal for Numerical Methods in Fluids, to appear, 1984.

{3} J.B. BELL and G.R. SHUBIN, "An Adaptive Grid Difference Method for Conservations Laws", J. of Comp. Physics 52, 569-591 (1983).

{4} M.J. BERGER, "Adaptive Mesh Refinement for Hyperbolic Partial Differential Equations", Stanford University, Report N°. STAN-CS-82-924.

{5} A. BRANDT, "Multi-Level Adaptive Solutions to Boundary-Value Problems", Math. of Computation, Vol. 31, N°. 138, April 1977, 333-390.

{6} A. BRANDT, "Multigrid Techniques : 1984 Guide with Applications to Fluid Dynamics", Lecture notes for the Computational Fluid Dynamics Lecture Series at the Von-Karman Institute for Fluid Dynamics, Rhode-Saint-Genese, Belgium, March 26-30, 1984.

{7} S.F. DAVIS and J.E. FLAHERTY, "An Adaptive Finite Element Method for Initial-Boundary Value Problems for Partial Differential Equations", Icase Report N°. 81-13, March 30, 1981.

{8} H.A. DWYER, "A Discussion of Some Criteria for the Use of Adaptive Gridding", AIAA Comp. Fluid Dynamics Conference, Danvers, Massachusetts, July 13-15, 1983.

{9} P.A. GNOFFO, "A Finite-Volume Adaptive Grid Algorithm Applied to Planetary Entry Flowfields", AIAA Journal, Vol. 21, N° 9, Sept. 1983.

{10} J.B. GREENBERG, "A New Self-Adaptive Grid Method", AIAA Comp. Fluid Dynamics Conference, Danvers, Massachusetts, July 13-15, 1983.

{11} A. HARTEN and J.M. HYMAN, "Self-Adjusting Grid Methods for One-Dimensional Hyperbolic Conservation Laws", J. of Comp. Phys., Vol. 50, 235-260 (1983).

{12} T. HOLST and D. BROWN, "Transonic Airfoil Calculations Using Solution-Adaptive Grids", AIAA 5th Computational Fluid Dynamics Conference, Palo Alto, California, June 22-23, 1981.

{13} A. JAMESON, "The Evolution of Computational Methods in Aerodynamics", Princeton University, MAE Report N° 1608.

{14} R. LOHNER, K. MORGAN and O.C. ZIENKIEWICZ, "An Adaptive Finite Element Method for High Speed Compressible Flow", University College of Swansea, C/R/479/84.

{15} K. NAKAHASHI and G.S. DEIWERT, "A Practical Adaptative Grid Methods For Complex Fluid Flow Problems", 9th Int. Conf. On Num. Meth. in Fluid Dynamics, June 25-29, 1984, CEN-Saclay, France, Springer-Verlag, to appear.

{16} RON-HO NI. "A Multiple Scheme for Solving the Euler Equations". AIAA Journal, Vol. 20, N° 11, November 1982.

{17} B. STOUFFLET, "Résolution Numérique des Equations d'Euler des Fluides Parfaits Compressibles par des Schémas Implicites en Eléments Finis", thèse 3ème cycle, Univ. P. et M. Curie, Paris VI, 1984.

{18} R.M. STUBBS, "Multiple-Gridding of the Euler Equations with an Implicit Scheme", 6th AIAA Conference on Fluid Dynamics, Danvers, Massachusetts, July 13-19, 1983.

{19} J.F. THOMPSON, "A Survey of Grid Generation Techniques in Computational Fluid Dynamics", AIAA Paper 83-0447.

{20} W.J. USAB, Jr., E.M. MURMAN, "Embedded Mesh Solutions of the Euler Equation Using a Multiple-Grid Method", 6th AIAA Computational Fluid Dynamics Conference, Danvers, Massachusetts, July 13-15, 1983.

{21} N.N. YANENKO, V.D. LISSEIKIN, V.M. KOVENIA, "The Method of the Solution of Gas Dynamical Problems in Moving Meshes", Lecture Notes in Physics, Vol. 91, pp 48-61, Springer-Verlag, New York (1979).

{22} Shah M. YUNUS and Mark S. SHEPHARD, "A Comment on the Effectiveness of Uniform Finite Element Refinements", I. J. for Num. Mesh. in Eng., Vol 20 N° 1, January 1984, P. 187-194.

Imprimé en France

par

l'Institut National de Recherche en Informatique et en Automatique